



Mapping the Shoreface of Coastal Sediment Compartments to Improve Shoreline Change Forecasts in New South Wales, Australia

M. A. Kinsela^{1,2} · D. J. Hanslow¹ · R. C. Carvalho^{3,4} · M. Linklater¹ · T. C. Ingleton¹ · B. D. Morris¹ · K. M. Allen¹ · M. D. Sutherland¹ · C. D. Woodroffe⁴

Received: 21 March 2019 / Revised: 16 April 2020 / Accepted: 1 May 2020 / Published online: 27 May 2020
© The Author(s) 2020

Abstract

The potential response of shoreface depositional environments to sea level rise over the present century and beyond remains poorly understood. The shoreface is shaped by wave action across a sedimentary seabed and may aggrade or deflate depending on the balance between time-averaged wave energy and the availability and character of sediment, within the context of the inherited geological control. For embayed and accommodation-dominated coastal settings, where shoreline change is particularly sensitive to cross-shore sediment transport, whether the shoreface is a source or sink for coastal sediment during rising sea level may be a crucial determinant of future shoreline change. While simple equilibrium-based models (e.g. the Bruun Rule) are widely used in coastal risk planning practice to predict shoreline change due to sea level rise, the relevance of fundamental model assumptions to the shoreface depositional setting is often overlooked due to limited knowledge about the geomorphology of the nearshore seabed. We present high-resolution mapping of the shoreface-inner shelf in southeastern Australia from airborne lidar and vessel-based multibeam echosounder surveys, which reveals a more complex seabed than was previously known. The mapping data are used to interpret the extent, depositional character and morphodynamic state of the shoreface, by comparing the observed geomorphology to theoretical predictions from wave-driven sediment transport theory. The benefits of high-resolution seabed mapping for improving shoreline change predictions in practice are explored by comparing idealised shoreline change modelling based on our understanding of shoreface geomorphology and morphodynamics before and after the mapping exercise.

Keywords Coastal geomorphology · Seafloor mapping · Sediment budget · Shoreface morphodynamics · Shoreline change

Communicated by Brian B. Barnes

Electronic supplementary material The online version of this article (<https://doi.org/10.1007/s12237-020-00756-7>) contains supplementary material, which is available to authorized users.

✉ M. A. Kinsela
michael.kinsela@environment.nsw.gov.au

¹ Water, Wetlands and Coasts Science, Department of Planning, Industry and Environment, Sydney, NSW, Australia

² Geocoastal Research Group, School of Geosciences, University of Sydney, Sydney, NSW, Australia

³ School of Life and Environmental Sciences, Deakin University, Warrnambool, VIC, Australia

⁴ School of Earth, Atmospheric and Life Sciences, University of Wollongong, Wollongong, NSW, Australia

Introduction

Beaches and dunes are elements of much broader coastal barrier depositional systems, which evolve through sediment exchanges between connected depositional environments that may also include rivers, estuaries and inlets; the shoreface; and adjacent barrier systems (Swift et al. 1991; Roy et al. 1994; Cowell et al. 2003a). Coastal barriers are highly valued for settlement and recreation and provide important habitats and ecosystem services for terrestrial, estuarine and marine species (Barbier et al. 2011; Lazarus et al. 2016). Severe storms impact beaches and coastal settlements around the world today (Castelle et al. 2015; Scott et al. 2016; Harley et al. 2017; Brenner et al. 2018), and exposure is expected to increase through this century and beyond as global sea level rise triggers the landward retreat of many shorelines (Fitzgerald et al. 2008; Nicholls and Cazenave 2010). Basic principles of coastal depositional systems imply that where

relative sea level rise occurs, shorelines will retreat landward unless a significant sediment supply exists to offset the effects of rising sea level (Curry 1964; Swift et al. 1991). The rate of shoreline retreat may exceed passive inundation (the ‘bathtub’ effect) as rising sea level enables the progressive loss of sediment by wave action from beaches to adjacent sediment sinks (Stive 2004). Any connected depositional environment that has available accommodation space to accumulate sediment freed from the beach and dunes during erosion is a potential sink. Sediment may be lost to estuaries (flood-tidal deltas) or ‘down-drift’ beaches via littoral transport, to back-barrier lagoons via overwash, to dunes via aeolian transport and to the nearshore seabed shaped by waves (the shoreface) via offshore-directed currents and gravity (Roy et al. 1994; Wright 1995). However, inherited morphodynamic processes may also oppose such losses. The shoreface provides a steady long-term sand supply to beaches via wave action in some settings (Cowell et al. 2003b; Schwab et al. 2013; Kinsela et al. 2016), for example, which might counter shoreline retreat for slow rates of sea level rise or even maintain shoreline progradation where the rate of supply exceeds the effect of sea level rise (Fruergaard et al. 2018).

Uncertainty in the inherited morphodynamic states of coastal depositional environments and how they might respond to rising sea levels is a key weakness of shoreline change predictions (Cowell and Thom 1994). Sea level constrains the morphology and evolution of the shoreface (Stive and de Vriend 1995) and flood-tidal deltas (Van Goor et al. 2003; Van Maanen et al. 2013), both of which can have surface areas and sediment volumes vastly exceeding that of the sub-aerial beach system. Only slight changes in their morphologies in response to rising sea level may thus imply significant sediment redistribution and shoreline migration (Cowell et al. 2003a). This scale disparity means that even modest uncertainty in the depositional response equates to large uncertainty in future shoreline change (Cowell et al. 2006). Despite being ubiquitous to barrier systems, shoreface morphodynamics remain poorly understood due to complex hydrodynamics and sediment transport, and morphological response rates that reduce to immeasurable across the lower shoreface (Niedoroda et al. 1984; Wright 1995; Cowell and Kinsela 2018). The sensitivity of shoreline change to shoreface evolution under rising sea level is expected to vary with setting. It might be higher in (typically steeper) accommodation-dominated (Swift et al. 1991) settings, where waves shape the shoreface well beyond the surf zone and sea level rise drives shoreface encroachment into pre-existing coastal physiography (Roy et al. 1994; Cowell et al. 1995; Wolinsky and Murray 2009). It is likely to be lower, however, in (typically flatter) supply-dominated settings where sediment transport is mostly landward during sea level rise and back-barrier deposition controls the rate of shoreline migration (Lorenzo-Trueba and Ashton 2014; Walters et al. 2014; Brenner et al. 2015).

A simple parameterisation of the shoreface response to sea level rise is often a principal component of shoreline change predictions in coastal management practice. Coastal erosion hazard planning zones in Australia are commonly determined using the ‘Bruun Rule’ (Kinsela and Hanslow 2013; Wainwright et al. 2014). The Bruun Rule predicts the encroachment of the beach into a pre-existing dune during sea level rise, based on a presumption that the shoreface seabed translates upward and landward in dynamic equilibrium with sea level rise, with shoreface accretion supplied by wave-driven erosion of the dune enabled by a raised sea level (Bruun 1962, 1983). The physical reasoning for an equilibrium shoreface profile has been reviewed previously (Wright 1995; Cowell et al. 1999) and remains an area of ongoing research (Ortiz and Ashton 2016; Aagaard and Hughes 2017). The theories follow numerous observations that sedimentary shorefaces on wave-dominated coasts often develop concave profiles that might reflect the time-averaged response of the substrate to the wave climate (Dean 1991). The Bruun Rule is an idealised model that is well known to be flawed in most real-world settings due to simplifying and restrictive assumptions, including homogenous coastal geomorphology, the prevalence of an equilibrium shoreface profile that adjusts instantaneously with sea level rise and the absence of along-shore sediment transport gradients (Bruun 1988). It simply considers one potential cross-shore sediment exchange that may influence shoreline change at intermediate to long time-scales (Stive 2004; Zhang et al. 2004).

Application of the Bruun Rule in coastal risk management and planning across a broad range of settings, notwithstanding and often ignoring its restrictive assumptions, prompted critical debate about its merits and the fundamental assumption of an equilibrium shoreface profile (Pilkey et al. 1993; Thieler et al. 1995, 2000; Cooper and Pilkey 2004). A theoretical equilibrium profile shaped by cross-shelf wave-driven sediment transport is likely rarely attained in reality due to local depositional controls (including inherited physiography) and complex, multi-dimensional and temporally varying shoreface sediment transport (Niedoroda et al. 1984; Wright 1995). Ongoing controversy around broad-scale application of the Bruun Rule and its inherent equilibrium profile assumption (Cooper et al. 2020) highlights the need to investigate uncertainties in shoreface geomorphology and morphologic response to sea level change at a local scale, to develop meaningful shoreline change predictions for complex geomorphic settings (Thieler et al. 1995, 2001; Miselis and McNinch 2006; Cooper et al. 2018). This is particularly true for embayed coasts where cross-shore sediment exchanges dominate barrier evolution and shoreline migration (Cowell and Kinsela 2018), and where the sum of sediment exchange between beach, shoreface and estuaries may significantly influence shoreline change relevant to coastal risk planning (Stive 2004).

Mapping coastal depositional systems is a fundamental step towards developing and formalising conceptual frameworks of coastal evolution to guide appropriate application of predictive models (Cowell et al. 2003a; French et al. 2016) that inform coastal risk assessment and planning (Hanslow et al. 2016; Kinsela et al. 2017). Knowing the dimensions, composition and morphodynamic state (relative to a theoretical equilibrium) of the shoreface could enable more robust shoreline change forecasts in complex geomorphic settings. While the shoreface is the seabed nearest to land, the coverage and detail of seabed mapping is often lower than that for deeper environments farther from shore (Linklater et al. 2019). That is because vessel-based mapping is more efficient in deep water (increased swath width), navigation in coastal waters is hazardous and necessitates smaller vessels with limited range and operating conditions, satellite and aerial imagery may be affected by wave breaking and water turbidity due to runoff and wave disturbance of the seabed and shallow coastal waters are often mapped to sufficient detail for navigation using low-resolution techniques. Mapping is usually limited to point soundings collected for navigation charts, with survey detail concentrated around ports and information about the seabed substrate limited. Recent advances in airborne lidar now provides an efficient means to map bathymetry and geomorphology in shallow coastal waters at a level of detail comparable to multibeam echosounders (Finkl et al. 2005; Kennedy et al. 2014).

We present high-resolution bathymetry and substrate mapping for a coastal sediment compartment in New South Wales (NSW), Australia (Fig. 1a). Seamless topographic-bathymetric airborne lidar data have been collected along the entire NSW coastline, and vessel-based multibeam echosounder (MBES) surveys cover deeper water in priority regions. The data include both elevation and signal intensity (lidar reflectivity and MBES backscatter) point clouds from which gridded elevation models and signal intensity mosaics are derived. Sediment grab samples are collected to ground-truth the remote sensing data and classify the coastal seabed to inform coastal and marine management applications (Linklater et al. 2019). The seabed mapping supports a new legislative framework to guide coastal risk management and planning, in which coastal dynamics within and between defined sediment compartments must be considered in managing coastal hazard risks. The sediment compartment hierarchy provides a template for understanding shoreline dynamics using principles of coastal depositional systems (Chapman et al. 1982; Thom et al. 2018), with a view to develop coastal sediment budgets (Komar 1996; Rosati 2005) and integrate cross-shore and alongshore shoreline modelling techniques with geological evidence to overcome the limitations of idealised approaches in complex geomorphic settings (Stive 2004; Cooper and Pontee 2006).

We apply the high-resolution seabed mapping data to investigate the sensitivity of the modelled ‘Bruun effect’ to our parameterisation of the geomorphology and morphodynamic state of the shoreface. Predicting the depositional response of the beach-shoreface system to sea level rise, and resulting shoreline change, requires an understanding of the present state of the coastal morphodynamic system and the spatial and temporal scales at which it responds to changing boundary conditions. Here, the Bruun effect (Stive 2004) refers to the translation response of an equilibrium shoreface to sea level rise, as expressed by the standard Bruun Rule (Bruun 1962, 1983). ‘Shoreface response’ refers to the vertical adjustment of the shoreface, whether under stable or varying sea level, noting that the response may be aggradation, deflation or null (i.e. statistically stationary through time). Importantly, lower shoreface response may vary from upper shoreface response due to inherited physiography and depth-dependent response timescales (Cowell et al. 1999; Cowell and Kinsela 2018). We characterise the ‘morphodynamic state’ of the shoreface by comparing observed profiles with theoretical equilibrium geometry using the nomenclature of Daley and Cowell (2013).

Regional Setting

New South Wales, Australia

The NSW coastline is oriented NNE-SSW and is roughly 1600 km alongshore (Fig. 1a) with 990 km of sandy shorelines forming 755 distinct beaches (Short 2007). The coast is situated on a passive tectonic continental margin that is relatively steep and narrow by global comparison, with a width to the shelf break of only 10–50 km, resulting in low attenuation of waves between deep water and the shore (Roy and Thom 1981). The shoreface and inner-continental shelf are steep, with the shoreface (to 30 m water depth) usually only a few kilometres wide and having a gradient of 0.43–1.28° (Boyd et al. 2004). The shoreface often has concave geometry where it has been surveyed in detail and is considered to extend to 30–40 m water depths depending on local wave climate and sediment (Cowell et al. 1999). Beyond the shoreface, a flatter (0.05–0.42°) inner-shelf plain often extends to wave base in around 60–70 m water depths (Boyd et al. 2004).

The coast is microtidal and wave dominated, experiencing a moderate-high energy wave climate with predominantly S-SE wave directions (Short 2020). Storm waves usually arrive from ESE to SE directions, and thus, larger headlands and promontories shelter beaches at the southern ends of coastal embayments, resulting in lower dune morphology. Infrequent storm waves from E to NE directions, however, mean that even sheltered beaches can be subject to severe erosion (Harley et al. 2017). Storm conditions are wave dominated (not surge

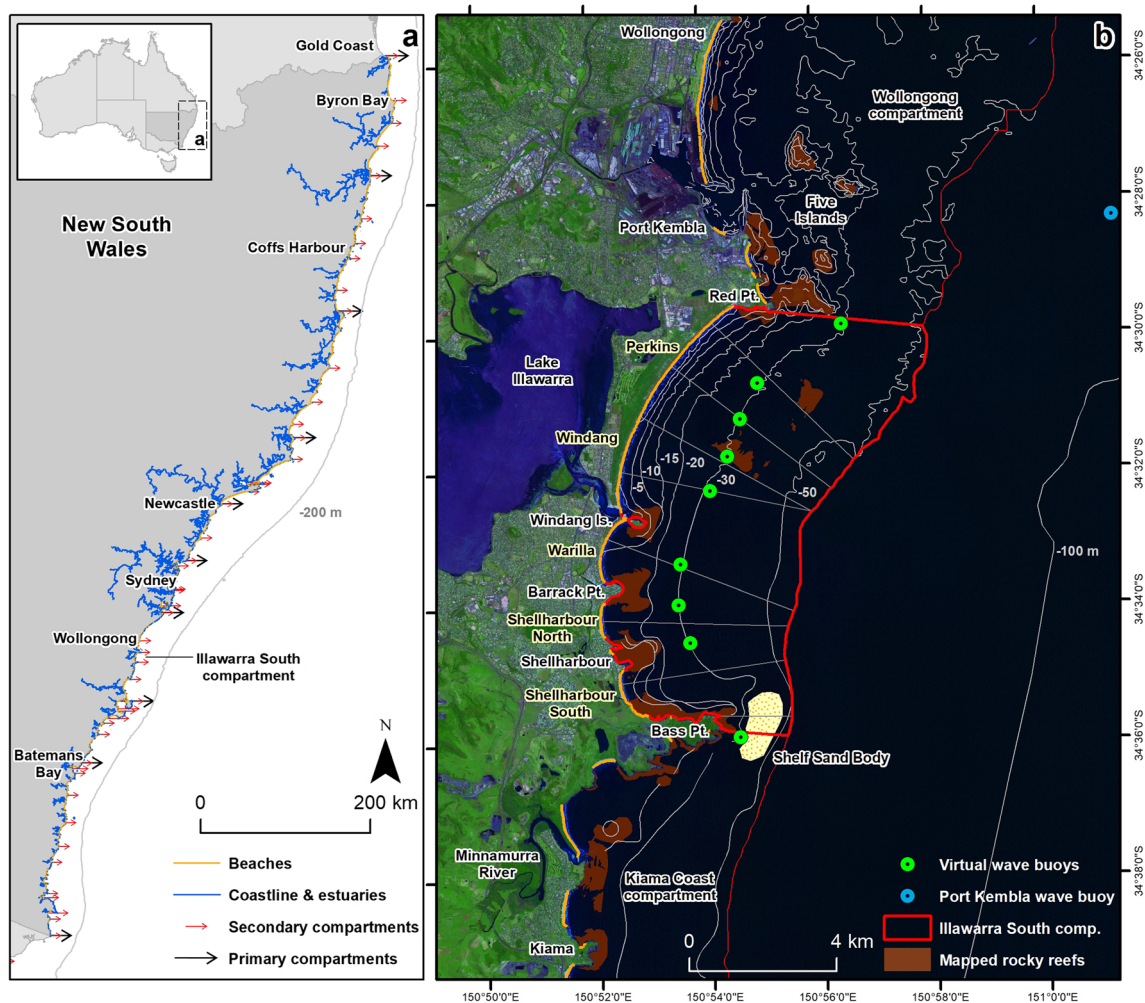


Fig. 1 Location map showing **a** the coastline and continental shelf of New South Wales with primary and secondary sediment compartment boundaries and **b** the Illawarra South compartment. Navigation bathymetry contours are shown with mapped rocky

reefs and the Bass Point shelf sand body. The Port Kembla deep-water wave buoy (80 m water depth) and virtual wave buoys (30 m water depth) used in this study are indicated, with eight shoreface-inner shelf analysis profiles (P1–P8) identified in subsequent figures

dominated) with extreme significant wave heights reaching $H_s = 9$ m, while storm-surge water levels rarely exceed 0.5 m. A threshold of $H_s > 3$ m distinguishes storm conditions from fair-weather conditions. Sediment movement is net northward due to the prevailing wave direction, although exchanges between beaches may be negligible or absent along the more embayed central to southern NSW coastline (Roy and Thom 1981; Short 2020). Coastal development behind some ocean and estuarine shores is presently at risk from beach erosion and tidal inundation, particularly during storms, and exposure is expected to increase with projected sea level rise (Cechet et al. 2012; Kinsela et al. 2017; Hanslow et al. 2018).

Illawarra South Compartment

We focus on the Illawarra South secondary sediment compartment located about 100 km south of Sydney (Fig. 1). The compartment is small, spanning 12 km in a straight line or

18 km alongshore from Red Point in the north to Bass Point in the south. It includes five major sandy beaches (Perkins, Windang, Warilla, Shellharbour North and Shellharbour South), a rocky shore cove (Shellharbour), a large coastal lake (Lake Illawarra) and a small tidal creek (Little Lake) located at the southern end of Warilla Beach (Short 2020). Perkins-Windang Beach is the longest sandy shoreline (6.8 km) and is located on a prominent Holocene coastal barrier between Red Point and Windang Island. The other major beaches are 1–1.5 km in length. Development is set back from the ocean shore by at least 300 m along Perkins-Windang Beach and is concentrated around the Lake Illawarra foreshore (Fig. 2a). Development occurs within 50 m of the ocean shore along the southern half of Warilla Beach where it is protected by a seawall (Fig. 2b). A water treatment plant limits development at Shellharbour North Beach, and a recreational marina complex is under construction behind Shellharbour South Beach (Fig. 2b).

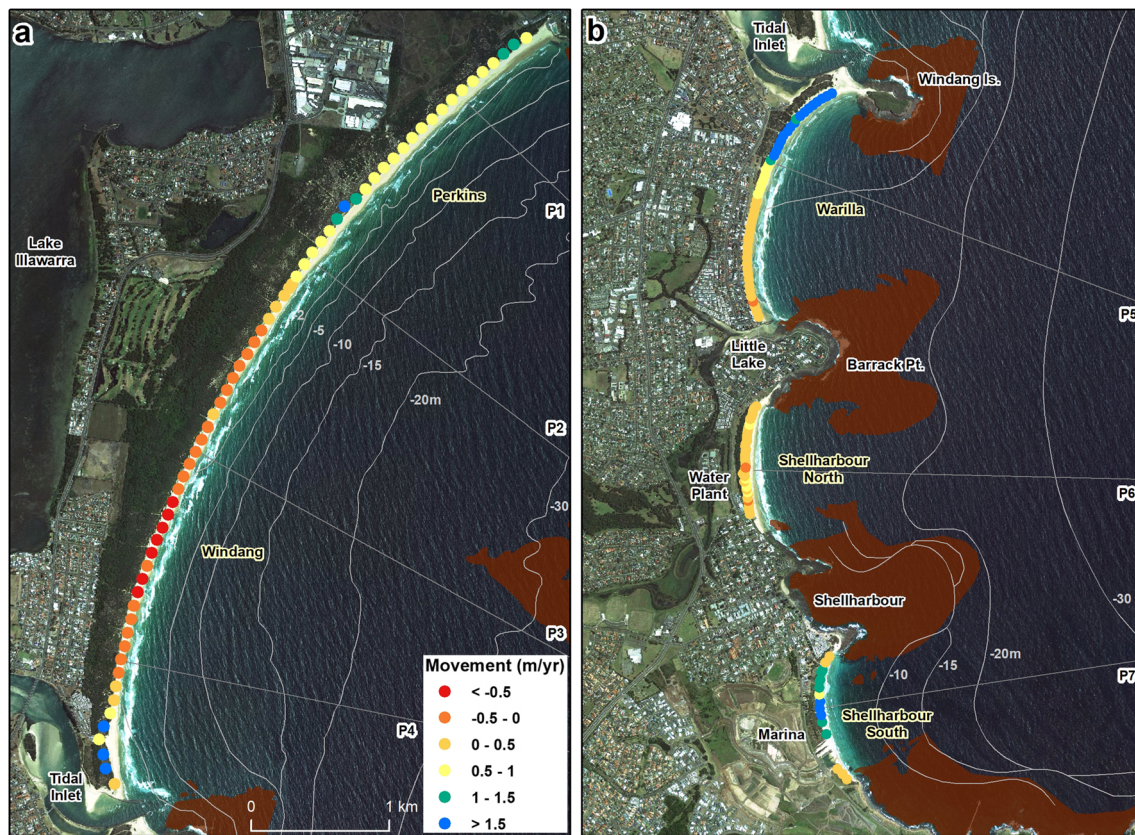


Fig. 2 Historical shoreline change (1980–present) from photogrammetry records at **a** Perkins-Windang Beach and **b** Warilla, Shellharbour North and Shellharbour South beaches. Markers show the average rate of

movement of the foredune face (2.5–4.5 m AHD elevation contour) with positive values indicating accretion and negative values indicating retreat. See Fig. 1 for beach locations

Existing navigation bathymetry shows that the shoreface is relatively steep with an average slope of 0.76° to 30 m water depth and 0.46° between 30 and 50 m water depths (Fig. 1b). The detail of navigation bathymetry is relatively high in the north of the compartment, near Port Kembla, and is lower in the south. A headland-attached shelf sand body of the type described by Field and Roy (1984) borders Bass Point. Rocky reefs previously mapped from aerial and satellite imagery extend out from rocky shores around all headlands (including Windang Island), and isolated outcrops occur on the shoreface off Perkins-Windang Beach (Fig. 1b). The longest ocean wave measurement record in Australia is located off Port Kembla (Fig. 1b), where wave buoys have been deployed since February 1974. The deep-water (80 m water depth) wave climate of the Illawarra region is described by a mean significant wave height ($\overline{H_s}$) of 1.6 m ($\sigma = 0.7$), mean significant wave period ($\overline{T_s}$) of 7.9 s ($\sigma = 1.6$), mean peak wave period ($\overline{T_P}$) of 9.6 s ($\sigma = 2.4$) and mean wave direction of 132° (mode = 161°). A regional wave model using WAVEWATCH III (NOAA, USA) with 100 m spatial resolution at 10 m water depth (Taylor et al. 2015) provides nearshore wave data at virtual buoy locations shown in Fig. 1b.

Methods

Geomorphology and Sediment Distribution

High-Resolution Seabed Mapping

We carried out high-resolution seabed surveys using an R2Sonic 2022 (200–400 kHz) MBES system. Survey speeds were 4–6 knots with 20–50% overlap between survey lines to achieve a minimum density of 4–5 soundings/m². Sound velocity data were recorded at the sonar head, and water column profiles were measured 2–4 times daily to correct for depth-dependent variability in sound speed. Vessel motion and position were measured by an onboard inertial motion unit and a POS MV (Applanix, Canada) system using G2 real-time satellite corrections. Motion data were post-processed for an improved vessel trajectory (RMSE < 0.03 m). Bathymetric soundings were pre-processed in Hypack (Xylem, USA), cleaned using CUBE modelling in Qimera (QPS, Netherlands) to International Hydrographic Organization (IHO) standard 1B and reduced to Australian Height Datum (AHD). The soundings were gridded using weighted averaging to produce a 5-m-resolution grid. Backscatter data were processed in Fledermaus FMGT (QPS, Netherlands) where

travel time, power, gain and beam angle corrections were applied. Backscatter values were adjusted (± 5 db) in overlapping transects where power settings varied to normalise the signal in adjacent areas. The MBES survey was carried out in May–November 2017 and covered 45 km² (72%) of the compartment seabed in water depths of 7–62 m (Fig. 3b).

Seamless topographic-bathymetric lidar data covering the entire NSW coastline were acquired by Fugro Australia Pty. Ltd. under contract to the NSW Government between July and December 2018. The total data coverage is 6863 km² and extends from the sub-aerial coast to water depths up to 49 m (> 30 m on average) depending on water clarity at the time of survey. Both Rieggl VQ-820-G and LADS HD-ALB sensors were operated during surveys. The Rieggl sensor covered land and shallow waters to 7 m water depth, while the LADS sensor covered all coastal waters surveyed. The lidar data provide seamless coastal topography and bathymetry to IHO 1B survey standard. Surveys used an air speed of 160 knots, altitudes of 1600–1800 ft and line spacing of 336 m (356 m swath) and have a minimum point coverage of 2 points/m² for the Rieggl system and 3.4×3.4 m for the LADS system. Data were reduced to AHD and quality assured using the QA4LIDAR tool (FrontierSI 2019). The Illawarra South compartment was surveyed on 5

September 2018, covering a combined land and water area of 47 km² to a maximum water depth of -39 m AHD including 30 km² (48%) of the compartment seabed (Fig. 3a).

About one quarter (16 km²) of the compartment seabed was mapped by both the lidar and MBES surveys, representing 36% of the total MBES survey area. The mean difference between the lidar and MBES bathymetry surfaces was 0.04 m (median < 0.005 , $\sigma = 0.33$), with a root mean square difference of 0.267 m. The resolution difference between the LADS and MBES data contributes to greater differences across rugged substrates, in particular. The consistency between the lidar and MBES surveys was satisfactory to develop an integrated high-resolution bathymetry model covering the entire compartment seabed. We used the Topo to Raster tool in ArcGIS 10.4 (ESRI, USA) to create a seamless 5-m-resolution surface and included existing navigation bathymetry data (Fig. 1b) beyond the survey area to ensure reliable interpolation across sediment compartment boundaries.

Sediment Sampling and Analysis

Seabed sediment samples were collected during 4–5 April 2018 using a Smith McIntyre grab deployed from RV

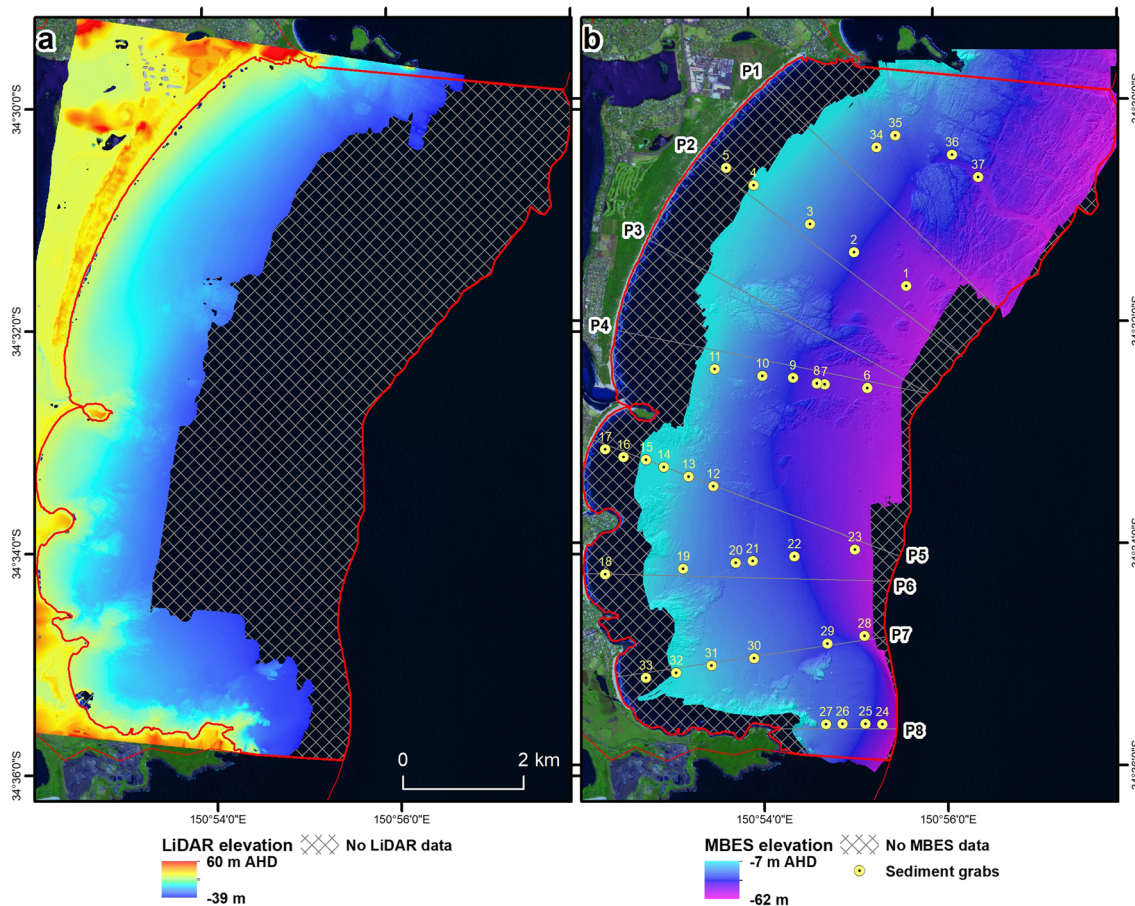


Fig. 3 High-resolution seabed bathymetry data from **a** airborne lidar and **b** multibeam echosounder (MBES) surveys. The locations of 37 seabed

sediment grab samples and eight cross-shelf analysis profiles (P1–P8) are indicated

Bombora. Sediment grabs were recovered from 37 sites in 6 to 50 m water depths across the range of backscatter return signal (Fig. 3b). Sediment grabs were photographed, sampled, inspected and described onboard, with further description carried out in the laboratory. Surface samples were collected from the upper 2 cm of each undisturbed grab and refrigerated in zip-lock bags. Samples were washed in the laboratory to extract salt, dried in an oven at 60 °C and subsampled for analysis. The first subsample was sieved at 0.5-phi intervals down to 0 phi. Sediment grains finer than 0 phi were measured by laser diffraction using Malvern Mastersizer 2000. Grain size statistics were calculated using the method of Folk and Ward (1957) in GRADISTAT software (Blott and Pye 2001). A second subsample was analysed for total carbonate content using the loss-on-ignition (LOI) method at 925 °C.

Seabed and Compartment Classifications

To quantify shoreface areas composed of hard (temperate rocky reef) and soft (sediment) substrates, we followed methods described by Linklater et al. (2019). We created a fine-scale (27 cell-radius window) Bathymetric Position Index (BPI) surface using the Geomorphometry and Gradient Metrics Toolbox v2.0 in ArcGIS 10.4, and a ruggedness surface (3-cell rectangular window) using the Benthic Terrain Modeler toolbox v3.0. Thresholds for differentiating seabed outcrops were identified through inspection and analysis of the raster statistics. Values above 0.4 in the BPI surface captured features interpreted as reef platforms, while values below -0.4 captured depressions within and around reef platforms. The classes were combined to form BPI reef area footprints. A ruggedness threshold of >0.0003 captured visible reef areas in the 5-m bathymetry surface. We combined rugged areas with the BPI reef area footprints to fill most narrow channels between raised reef platforms that were not identified as raised outcrops by the BPI analysis alone. Surf zone bars captured by the BPI analysis (having comparable BPI values to reef platforms) were identified and removed using a water depth threshold of -7 m AHD. Reef areas were converted to polygons, and remaining holes were removed using the Eliminate Polygon Parts tool. Some manual cleaning was carried out to remove remaining erroneous areas such as the steep lower face of the Bass Point shelf sand body.

We created a provisional sediment distribution map for the compartment based on our interpretation of the intensity (backscatter and reflectivity) data informed by our sediment sampling results. Using a supervised classification method (Linklater et al. 2019), we classified the seabed intensity data for areas not identified as rocky reef into four classes that reflect the combined influences of sediment texture and composition on the return signals. Although the sediment classes do not always reflect distinct facies (which may be indistinguishable in the intensity data alone), they capture the

distribution of key sediment textures described by our remote sensing and sediment sampling, which we then interpret within the context of water depth and geomorphic setting.

Our high-resolution mapping and seabed classifications provide an opportunity to revise previous interpretations of tertiary compartment and sub-compartment boundaries within the Illawarra South secondary compartment (Carvalho et al. 2017; Kinsela et al. 2017) to guide sediment budgeting and shoreline change modelling. We consider the orientation and exposure of beaches and headlands, visible alongshore sediment transport pathways, inner-shelf sediment distributions and shoreface morphodynamics. Whereas secondary compartments identify depositional system connectivity at intermediate timescales (decades to centuries), tertiary compartments and sub-compartments provide practical templates for developing sediment budgets to model the depositional responses of beach-shoreface systems (Thom et al. 2018).

Shoreface Morphodynamics

We consider two aspects of shoreface morphodynamics that might influence coastal sediment budget response to sea level rise: the present *morphodynamic state* of the shoreface and the extent of the *active zone*, which is the shoreface area that is morphodynamically active over the intermediate timescales of interest (i.e. several decades to centuries). Figure 4 defines the parameters used to describe the domains and dimensions of the shoreface profile. In our setting, the shoreface often adopts a concave shape due to the dominance of depth-dependent cross-shelf sediment transport by shoaling waves. The surf zone has a flatter average grade to the breakpoint bar that is controlled by breaking waves and is a superimposed profile that fluctuates at short timescales.

Morphodynamic State

Shoreface profiles can reflect a balance between onshore and offshore sediment transport that varies with wave climate and sediment type (Dean 1991; Wright 1995; Cowell et al. 1999), which develops to varying degrees within the overriding boundary condition of the inherited physiography (Thieler et al. 1995). The shoreface morphodynamic state can be classified as *overfit* (shallower than equilibrium), *underfit* (deeper than equilibrium) or *graded* (profile consistent with equilibrium geometry) by comparing a measured profile with the theoretical equilibrium geometry for that setting (Cowell et al. 2003b; Daley and Cowell 2013). These conditions are characterised by negative, positive and neutral sediment accommodation potential, respectively. The depositional implications during sea level rise are such that an overfit shoreface is unlikely to be a sink for coastal sediment (and may be a source if the net direction of transport is onshore), an underfit shoreface is a potentially vast sink that might sequester sediment from the beach (if the net direction of

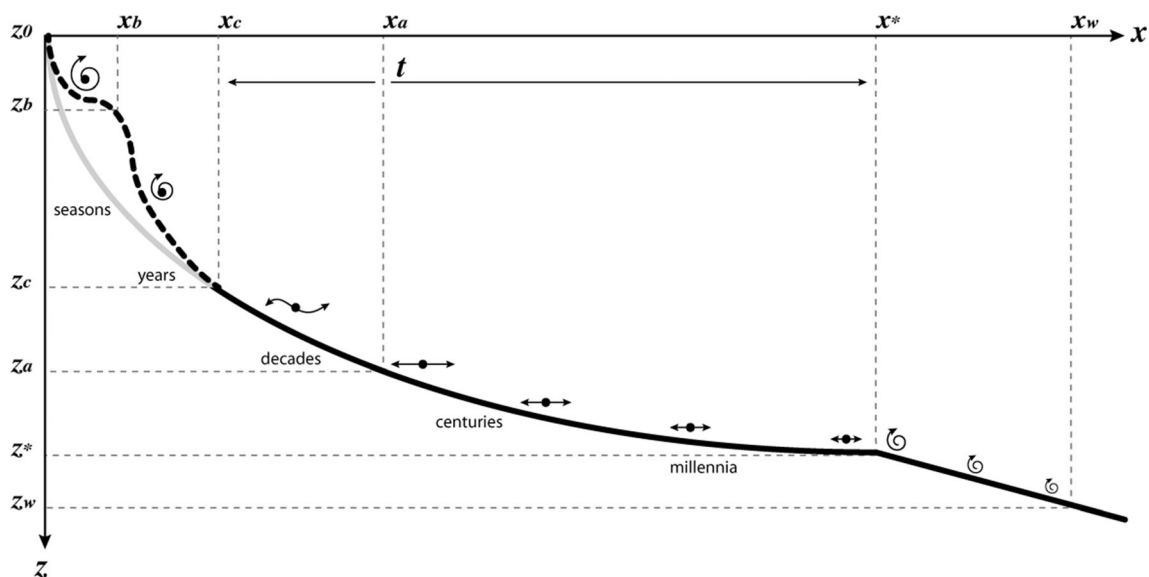


Fig. 4 Shoreface-inner shelf profile definitions. The upper (z_c), active (z_a) and lower (z_*) shoreface depth limits are shown relative to the shoreface origin (z_0) and wave base (z_w). The cross-shore scale of the shoreface (z_0 to z_*) is emphasised relative to the inner-shelf plain (z_* to z_w). The surf zone profile (dashed) is influenced by breaking waves shoreward of the

breakpoint bar (z_b). Timescales (t) of shoreface profile adjustment reflect depth-dependent rates of wave-driven sediment transport as illustrated by the qualitative motion of sediment grains at the seabed. Adapted from Cowell and Kinsela (2018)

transport is offshore) and a graded shoreface is a potential sediment sink that might grow in proportion with sea level rise.

To assess the morphodynamic state of the shoreface throughout the compartment, we extracted depth profiles from our high-resolution compartment bathymetry model along eight representative shore-perpendicular transects (Fig. 3b). Profiles P1–P4 capture variation in shoreface profile geometry along Perkins-Windang Beach, while the profiles at Warilla (P5), Shellharbour North (P6) and Shellharbour South (P7) beaches capture variation between embayments. Profile P8 captures the contrasting morphology of the Bass Point shelf sand body. We also derived depth profiles from the navigation bathymetry data (Fig. 1b) for comparison. Shoreface profiles extracted from the high-resolution bathymetry model were compared to the theoretical equilibrium profiles described by Dean (1991), hereafter DN91 profiles, and Ortiz and Ashton (2016) after Bowen (1980) and Bagnold (1963), hereafter OA16 profiles. While others have used functions of the form $z = ax^m$ to describe equilibrium profiles, we recognise Dean's (1991) synthesis and calibration of the function to profile and sediment data from the surf zone and upper shoreface. In contrast, the OA16 profiles balance onshore- and offshore-directed wave-driven sediment transport across the wave shoaling zone and, therefore, should be more representative of the broader shoreface geometry.

To derive a DN91 equilibrium profile for our setting, we used a scaling coefficient consistent with medium quartz sand ($a = 0.11$) and an exponent ($m = 2/3$). To calculate OA16 equilibrium profiles for each location (P1–P8), we used deep-water wave data from the long-term Port Kembla wave buoy record (1974–2019), transformed nearshore wave data at each profile based on the shorter directional wave buoy record (2012–2019) and sediment

fall velocities (w_s) corresponding to median grain sizes (D_{50}) from grab samples retrieved in 20 m water depth near each profile. We derived *morphodynamic* wave periods following Ortiz and Ashton's (2016) methods of $T_0 = 9.6$ s (also consistent with $\overline{T_p}$ at the Port Kembla buoy) and $T_0 = 10.9$ s, based on wave climate weightings of H^5 (W1) and $H^5 T^{-5} \sin^{-5}(kz)$ (W2) respectively. The weightings scale the two-dimensional wave height-period histogram that is used to derive morphodynamic wave climate parameters that affect evolution of the shoreface profile. Equilibrium shoreface-inner shelf profiles were then derived using the local morphodynamic wave period and sediment fall velocity. Additional description of our derivation of theoretical equilibrium profiles and morphodynamic wave climate parameters is provided in the [supplementary material](#).

Active Zone

We use 'active zone' after Stive and de Vriend (1995) to describe the part of the shoreface profile that maintains statistically stationary geometry over the timescale of interest (Fig. 4). Morphological response rates are equal to or exceed the rate of sea level change in the active zone, implying that profile geometry is maintained (in a time-averaged sense) during sea level rise, and profile response may follow the Bruun effect (Cowell and Kinsela 2018). The active zone extends from the shoreface origin (z_0) to the active shoreface limit (z_a). Locating z_a therefore provides a means to estimate the *potential* shoreface sediment accommodation volume generated by sea level rise for a given rate of sea level change. The actual depositional response will depend on local shoreface geomorphology and the

morphodynamic state of the profile (i.e. overfit, underfit or graded), with cross-shelf sediment transport potential and shoreface response decreasing with increasing water depth to negligible (at intermediate timescales) around the lower shoreface limit (z_*).

We estimate the upper (z_c) and lower (z_*) shoreface depth limits (Fig. 4) using Hallermeier's (1981) limits of profile adjustment (d_l) and significant cross-shelf sediment transport (d_s), respectively. We calculate regional (compartment) and local (profiles P1–P8) values of z_c and z_* using deep-water (Port Kembla buoy) and nearshore (virtual buoy) wave climate data, respectively, and sediment grain size data from our grab samples (see the [supplementary material](#)). Hallermeier's formulae estimate the seaward limits of measurable wave shaping of the nearshore profile (d_l) and significant wave-driven cross-shelf sediment transport (d_s) at an *annual* timescale. Thus, z_c and z_* should provide inner and outer bounds for z_a at intermediate timescales—i.e., the limit of significant shoreface response to sea level rise over decades to a few centuries should be between the limit of observable profile response to wave conditions during any particular year and the limit of non-negligible wave-driven cross-shelf sediment transport. In exploratory modelling, Cowell and Kinsela (2018) found that for steady (or time-averaged) rates of sea level change, z_a converged on a depth reflecting the balance between local morphological response rates and the rate of sea level change. Specifically, z_a approached d_l for slow (0.5 mm/year) rates of sea level change or averaged over long timescales (millennia) and converged on d_s for fast (5 mm/year) rates of sea level change or over short timescales (years).

Empirical evidence of lower shoreface response timescales and z_a rarely exists as accurate repeat surveys of shoreface bathymetry (from the surf zone to z_*) covering multiple decades are required to observe profile change beyond z_c (e.g. Patterson and Nielsen 2016). In the absence of long-term repeat bathymetric survey data for the Illawarra South compartment, we apply Ortiz and Ashton's (2016) morphodynamic depth of closure (MDOC) method to estimate z_a at a 100-year timescale. Their approach uses energetics-based formulae for wave-driven sediment flux and morphodynamic wave climate parameters to calculate theoretical surface response timescales across the shoreface profile. We calculate a regional z_a using long-term deep-water wave data (Port Kembla buoy), and local z_a in 30 m water depth (virtual buoys) adjacent to profiles P1–P8 (Fig. 1b). Our calculations of regional and local z_a (MDOC) are provided in the [supplementary material](#).

Shoreline Change Analysis

Historical

Photogrammetry records exist for many NSW beaches and provide a useful measurement record for investigating historical beach change, with aerial photographs captured every several years since the 1940s in most locations (Hanslow

2007). We compared historical beach behaviour by tracing the movement of the elevation contour marking the frontal dune face (2.5–4 m AHD depending on shoreline exposure) during 1980–2018 using the NSW Beach Profile Database (Harrison et al. 2017). We restricted our analysis to that period to avoid inaccuracies and artefacts in photogrammetry data prior to 1970 (Hanslow 2007), influences from human interventions (e.g. Doyle et al. 2019a) and the impacts of a series of particularly severe storms during the 1970s.

Future

We evaluate the potential benefits of high-resolution seabed mapping for coastal risk management and planning through idealised modelling of the sediment budget implications of potential shoreface response to sea level rise on future shoreline change. For the purpose of that exercise, we assume the shoreface response is the only sediment budget response to sea level rise. While the embayed setting suggests alongshore sediment sharing between the four sandy beaches is limited, we ignore that and other potentially significant sediment budget components, such as the response of the Lake Illawarra flood-tidal delta to sea level rise (Van Goor et al. 2003) and changes in carbonate sediment balance (Simeone et al. 2018). We consider a 1-m sea level rise as a nominal scenario as our purpose is only to investigate the sensitivity of predicted shoreline change to our parameterisation of shoreface geomorphology and morphodynamics. While that value lies towards the upper end of 'likely' range Intergovernmental Panel on Climate Change projections for 2100 (Oppenheimer et al. 2019), others suggest that the potential for accelerated ice losses means that a 1-m sea level rise lies well within the uncertainty range for risk assessment (Le Cozannet et al. 2017; Sweet et al. 2017). Our results are comparative only and should not be considered as rigorous predictions of future shoreline change.

We first apply the standard Bruun Rule at representative profiles along each beach as has been done in practice to assess future shoreline response to sea level rise in the Illawarra South compartment (Cardno 2010; SMEC 2010) and elsewhere in Australia (Kinsela and Hanslow 2013; Wainwright et al. 2014). We do that for P1–P7 (Fig. 2) using two shoreface profiles at each location: (1) a profile based on navigation bathymetry data (Fig. 1b) to reflect applications in practice and (2) a profile derived from our high-resolution bathymetry model. We compare Bruun Rule predictions based on closure depths of the upper (z_c), active (z_a) and lower (z_*) shoreface limits for each profile. Our comparison is intended to evaluate the sensitivity of shoreline change predicted by the Bruun Rule to (1) alongshore variation in shoreface geometry, (2) profile closure depth and (3) the detail to which the available bathymetry data captures shoreface geometry. In this simple *profile* approach, each profile (P1–P7) is essentially considered to be an independent beach-shoreface system.

Later in the discussion, we demonstrate a *compartment* approach to predicting shoreline change, again using the Bruun Rule as a simple model of shoreface response to sea level rise, but applying it at Perkins-Windang Beach using insights on sediment transport potential from our analysis of shoreface geomorphology and morphodynamics. In that example, we use the high-resolution seabed mapping to account for the effects of shoreface reef outcrops and alongshore variation in shoreface geometry on the predicted beach-shoreface sediment exchange in response to sea level rise.

Results

Geomorphology and Sediment Distribution

Our high-resolution bathymetry model (Fig. 5a) captures the compartment seabed in unprecedented detail, revealing a shoreface-inner shelf that is more complex than was previously

known (Fig. 1b). The BPI surface (Fig. 6a) identifies rocky reefs and distinguishes exposed platform surfaces (red) from interstitial channels (blue) that may be partially sediment filled. In the northeast, a large reef platform extends from Red Point to the offshore extent of our survey and is contiguous into the Wollongong compartment to the north (Fig. 3b), covering the inner-shelf off the northern third of Perkins-Windang Beach beyond 40 m water depth. The platform is divided by a prominent sinuous palaeo-drainage channel. The central compartment seabed has patches of rocky reef outcropping between 20 and 50 m water depths, the largest being an oval-shaped feature located off Windang Beach that measures 3 × 1.3 km. Fringing reef platforms extend from rocky shores around Windang Island, Barrack Point, Shellharbour and Bass Point into 25–30 m water depths, while the seabed beyond is predominantly sedimentary plains. The ruggedness analysis (Fig. 6b) describes reef texture and differentiates rugose outcrops from smoother platforms and patchy sediment veneer. Rocky reefs cover 20.67 km² (33%) of the total seabed area (62.32 km²),

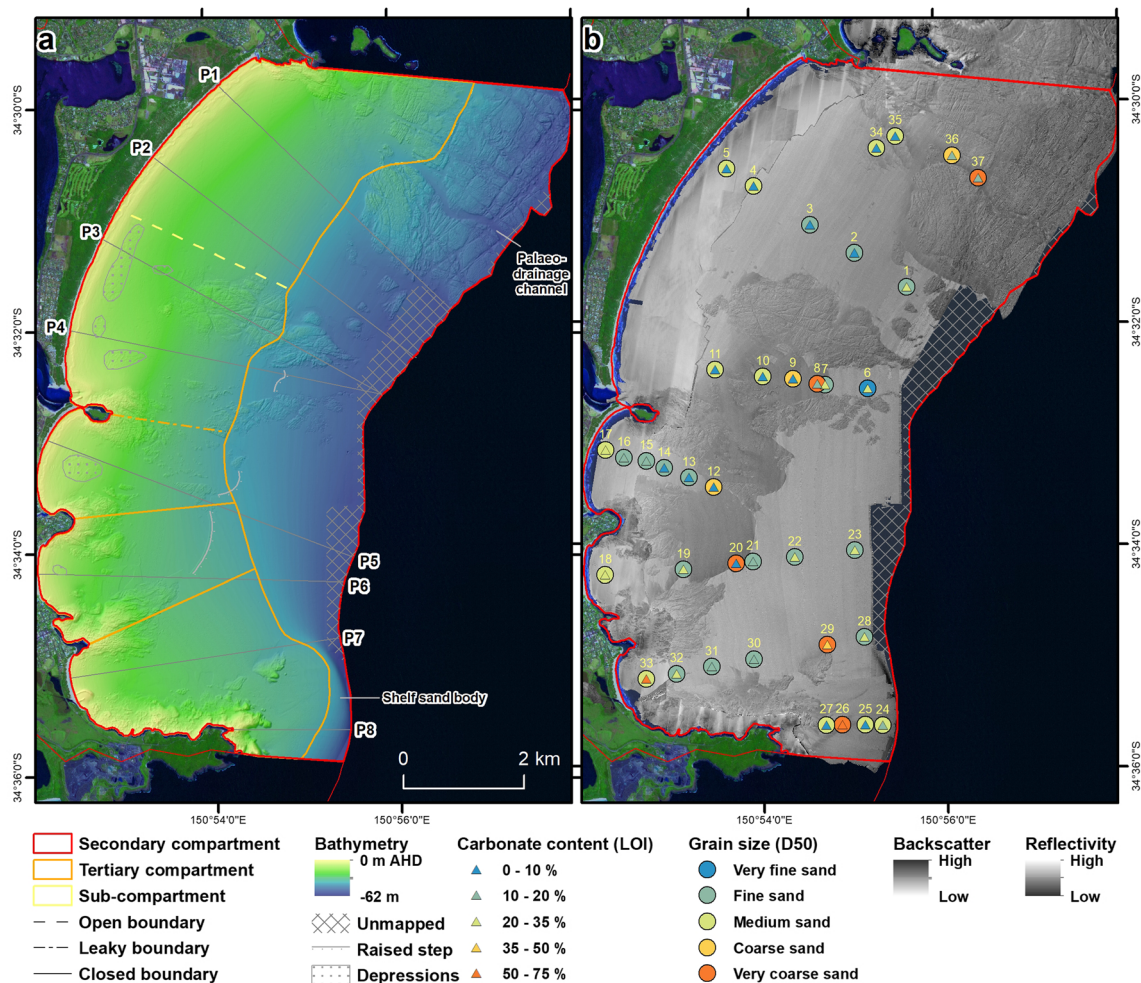
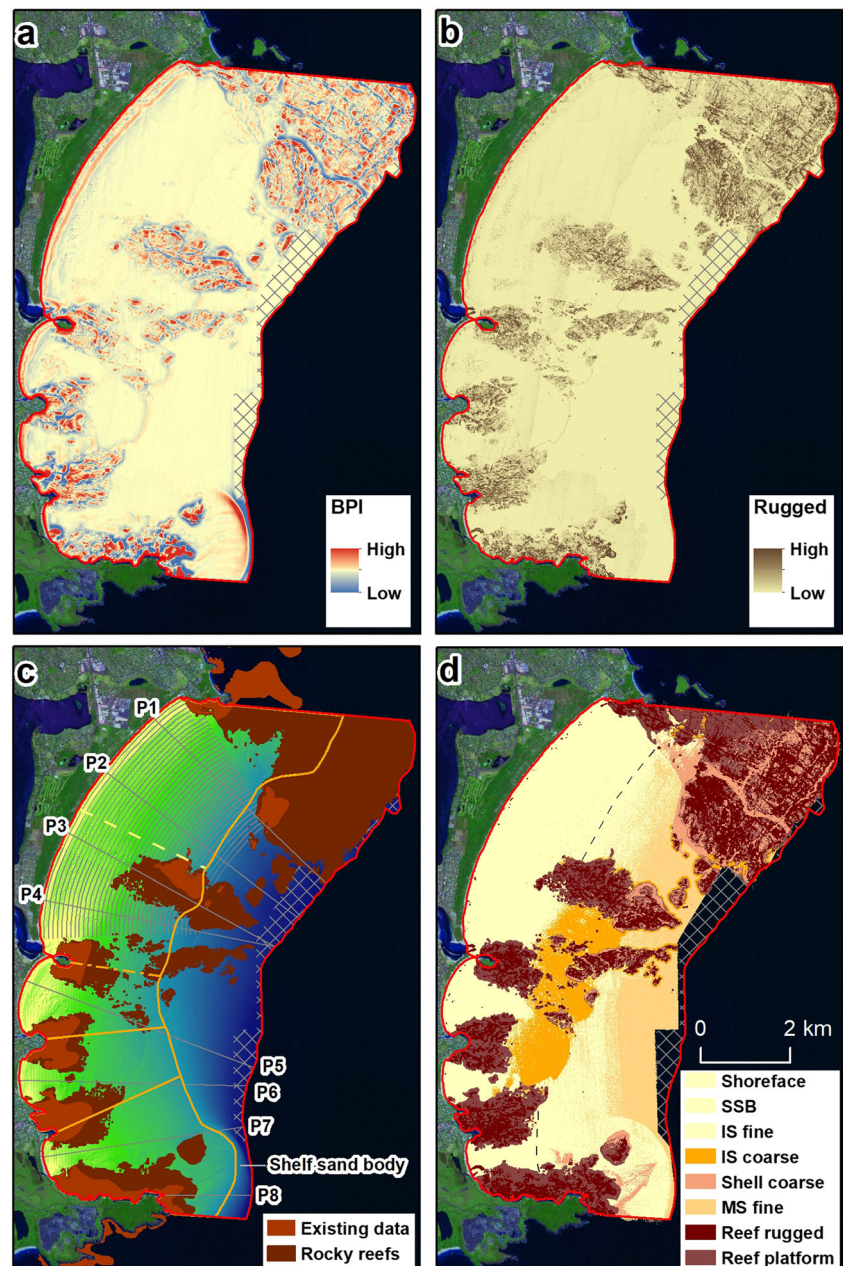


Fig. 5 High-resolution seabed mapping results: **a** integrated compartment bathymetry model, and **b** the texture (D_{50}) and carbonate content (LOI) of sediment grab samples overlain on MBES backscatter

and lidar reflectivity mosaics. Laboratory analysis results for the grab samples are provided in Table 1. Our compartment classification in **a** shows tertiary compartment and sub-compartment boundaries

Fig. 6 **a** Bathymetric Position Index (BPI) and **b** ruggedness analysis surfaces derived from the high-resolution bathymetry model (Fig. 5a). **c** Rocky reefs mapped by our seabed classification compared with existing mapping. Shore-parallel contours (every 5th contour shown) used to create alongshore-averaged shoreface profiles within the Perkins-Windang tertiary compartment (Fig. 9) are shown with our compartment classification (Fig. 5a). **d** Preliminary substrate map showing distributions of shoreface, shelf sand body (SSB), inner-shelf (IS), shell and mid-shelf (MS) sand types. Dashed lines approximate the gradations between shoreface sand and IS fine sand, which are indistinguishable in the backscatter data (Fig. 5b)



indicating that the compartment seabed is sediment dominated (Fig. 6c). Despite the occurrence of rocky reefs, only 8.3% of the shoreface to 30 m water depth off Perkins-Windang Beach was classified as rocky reefs. The smoother seabed between reef platforms is sedimentary plains, which were the focus of sediment sampling (Fig. 5b). The sedimentary plains grade steadily with decreasing concavity across the shoreface-inner shelf with an average gradient of 0.82° to -30 m AHD and of 0.52° between -30 and -50 m AHD.

The backscatter intensity signal varies both gradually and abruptly within the sedimentary plains and correlates with changes in sediment texture and composition revealed by the grab samples (Fig. 5b). Median grain size grades from

medium ($> 250 \mu\text{m}$) to fine ($200\text{--}250 \mu\text{m}$) sand from the upper to lower shoreface off Perkins Beach near P2 (Table 1), where the backscatter data indicates continuous shoreface-inner shelf sediment cover. Carbonate content is low ($< 10\%$) from the upper shoreface to at least 40 m water depth. The fine sand in 50 m water depth (sample 1) is distinctly different from the fine sand in samples 2 and 3, having finer texture and higher carbonate content (Table 1). It also has a dark olive grey colour that contrasts with the mid-brown to increasingly fawn colours of samples 2 to 5. The backscatter signal off Shellharbour South Beach near P7 shows similar gradual variation that suggests a gradation in sediment character. Grain size is again seaward fining with increasing water

Table 1 Summary of sediment grain-size and carbonate content (loss on ignition, LOI) analysis results for grab samples retrieved from the Illawarra South compartment (Fig. 5b)

ID	Elevation (m)	Mean (μm)	Sorting	Skewness	Kurtosis	D_{10} (μm)	D_{50} (μm)	D_{90} (μm)	LOI (%)
1	-49.8	135	2.117	-0.072	1.388	57	136	322	29.3
2	-39.6	218	1.542	-0.035	0.952	127	220	378	8.2
3	-30.0	234	1.444	-0.001	0.981	144	235	377	6.8
4	-20.0	267	1.446	-0.014	0.987	165	266	434	8.6
5	-12.5	276	1.452	-0.014	0.984	174	275	449	9.2
6	-49.2	81	2.830	-0.472	1.666	14	103	213	30.6
7	-44.3	129	2.068	-0.188	1.490	56	131	273	23.5
8	-44.2	1036	1.767	-0.019	1.072	528	1046	1939	15.5
9	-40.4	637	1.542	0.062	1.087	379	642	1153	4.5
10	-34.6	429	1.584	-0.064	1.005	240	435	749	7.3
11	-24.7	478	1.593	-0.083	0.969	260	488	862	3.9
12	-31.3	602	1.543	0.052	1.056	363	603	991	4.5
13	-25.8	213	1.516	-0.016	0.961	128	214	350	7.2
14	-20.0	203	1.524	-0.001	0.967	119	203	339	9.6
15	-15.0	198	1.484	-0.020	0.955	120	198	326	14.3
16	-10.2	200	1.543	0.015	0.973	115	199	341	15.7
17	-6.0	294	1.611	0.041	0.967	159	290	556	27.1
18	-10.6	274	1.531	0.002	0.972	154	273	469	21.3
19	-27.5	157	1.609	0.007	0.935	88	157	300	30.7
20	-33.9	1108	1.964	-0.487	1.813	254	1252	1901	5.5
21	-34.9	154	1.602	0.009	0.938	86	154	293	17.7
22	-39.7	139	1.600	0.006	0.989	73	139	247	25.9
23	-50.1	147	1.743	-0.126	1.130	71	148	280	30.9
24	-45.6	408	1.582	0.082	1.043	236	402	709	18.9
25	-39.5	382	1.488	0.056	1.027	233	376	645	8.9
26	-34.8	1163	2.540	-0.055	1.058	352	1248	3643	59.0
27	-32.9	325	1.394	0.056	1.007	210	321	488	8.1
28	-49.8	212	1.653	-0.079	1.007	106	215	398	25.8
29	-38.7	852	2.204	-0.260	0.849	281	1016	1945	41.8
30	-30.0	199	1.529	-0.002	0.962	114	199	336	14.9
31	-25.1	225	1.507	-0.011	0.969	134	227	385	13.7
32	-20.2	227	1.509	-0.019	0.970	134	229	391	20.7
33	-13.0	301	1.632	0.015	0.945	159	300	584	53.5
34	-32.4	483	1.836	0.064	1.038	228	477	1046	3.1
35	-33.7	492	1.711	0.008	1.040	256	494	944	2.6
36	-39.7	910	1.653	0.050	0.844	488	881	1763	13.7
37	-45.2	1176	1.474	-0.182	0.901	684	1216	1842	12.3

The 10th (D_{10}), 50th (D_{50} , median), and 90th (D_{90}) percentile grain sizes are included, with the elevation of samples relative to Australian Height Datum (approximately mean sea level)

depth from samples 33 to 30. Carbonate content is much higher than the Perkins shoreface, exceeding 50% in 13 m water depth (sample 33) and decreasing offshore (Fig. 5b). The anomalous sample 29 in 39 m water depth comprising very coarse shelly sand was retrieved from a small area of high backscatter return surrounding a rocky reef outcrop. The comparison between samples 1, 6 and 23 retrieved from around 50 m water depth shows that they are very similar in texture

(103–148 μm) and carbonate content (~30%), and all were slightly cohesive and had suspended mud in sample water. In contrast, sample 28 from similar water depth is coarser (215 μm), has lower (26%) carbonate content and has a mid-brown colour that is more consistent with shoreface samples 30 and 31. The sedimentary shorefaces of Perkins and Shellharbour South beaches have notably smooth surface texture with no evidence of bedforms captured in the surveys.

In contrast to Perkins and Shellharbour South beaches, the backscatter signal across the shoreface-inner shelf off Windang, Warilla and Shellharbour North beaches transitions sharply from moderate (mid grey) to high (dark grey) around 25 m water depth, before returning to moderate at an abrupt discontinuity in 45 m, 40 m and 35 m water depths, respectively, that coincides with a 0.5-m raised step up to the finer sand beyond (Fig. 5). Except for the medium sand at sample 17, which was the shallowest grab retrieved (6 m water depth), the shoreface sand above 25 m water depth across the Warilla shoreface is notably finer (c. 200 μm) relative to the other beaches. Sample 18 from 10 m water depth off Shellharbour North Beach was comparable to sample 17, a depth at which fine sand was found off Warilla Beach (sample 16). Shoreface sand was not sampled above 25 m water depth off Windang Beach. Nonetheless, it is evident that the medium to fine sand on the upper to mid-shoreface south of Windang Island has consistently higher carbonate content than off Perkins Beach. The mid-shorefaces off Windang and Warilla beaches feature irregular scour depressions in 9–16 m water depths that are 25–50 m across and up to 0.5 m deep, and 50–150 m across and up to 1 m deep, respectively. In the high-intensity backscatter region beyond about 25 m water depth, sediment grabs returned coarse to very coarse quartz sand (600–1100 μm), orange in colour and with consistently low carbonate content in the sand fraction despite containing coarser shells and shell fragments. Medium sand samples 10 and 11 off Windang Beach have similar appearance and composition but are slightly finer in texture. Seaward of the raised step and abrupt discontinuity in backscatter signal, samples 7, 21 and 22 returned fine to very fine sand that has texture, carbonate content and colour somewhere between the fine sand from the Perkins (samples 2 and 3) and Shellharbour South (samples 30 and 31) lower shoreface-inner shelf and the finer sand farther from the shore (samples 1, 6 and 23).

The palaeo-drainage channel dissecting the large reef platform in the northeast of the compartment has a high backscatter signal and was found to contain coarse to very coarse iron-stained sand with abundant iron-stained quartz grains and granules with coarser shells and shell fragments (samples 36 and 37). The medium quartz sand (samples 34 and 35) is very similar to that found off Windang Beach (samples 10 and 11) where the backscatter signal was comparable (Table 1). The Bass Point shelf sand body has a moderate backscatter signal, which samples 24, 25 and 27 indicate is medium quartz sand (300–400 μm) with low carbonate content. Narrow channels of high-intensity backscatter signal trending southwest-northeast downslope contain very coarse sand (1248 μm) with high carbonate content in the form of abundant coarse shell fragments (sample 26).

Shoreface Morphodynamics

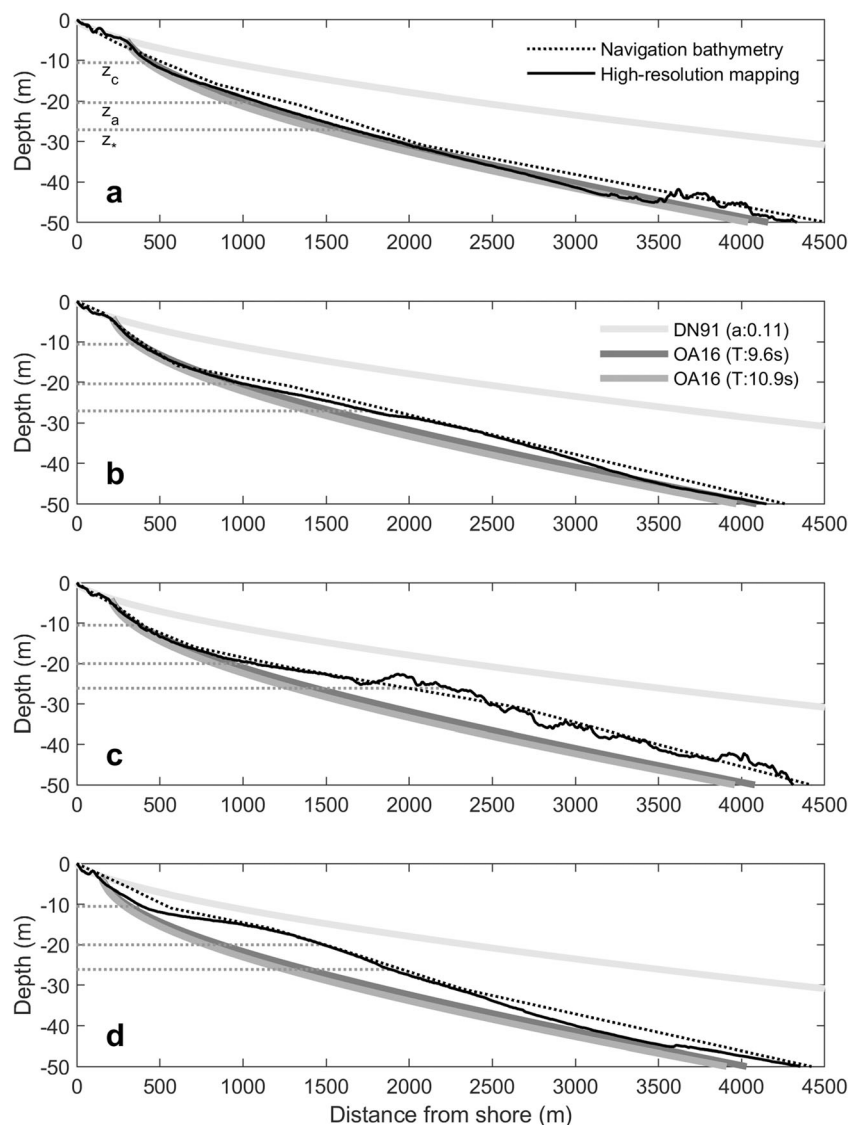
Morphodynamic State

Figure 7 compares shoreface profiles along Perkins-Windang Beach (P1–P4) based on navigation bathymetry contours (Fig. 1b) and our high-resolution bathymetry model (Fig. 5a) with the DN91 and OA16 equilibrium profiles. The contours capture the broad geometry of the shoreface-inner shelf seabed but provide no indication of seabed texture and local complexity. While the upper shoreface (to z_c) beyond the surf zone is concave along the beach, the lower shoreface-inner shelf geometry varies between profiles. P1 has a fine concave to linear geometry, while P2 has similar shoreface geometry to about 25 m water depth where a moderate convexity occurs. Profile P3 indicates that the large reef outcrop off Windang Beach influences shoreface geometry in that region beyond about 20 m water depth, where the surveyed shoreface deviates considerably from the OA16 profiles to meet the exposed reef platform. In 30 m water depth, the reef outcrop rises about 5 m higher than the sedimentary seabed between P1 and P2. Profile P4 features a prominent but smooth convexity across the mid-lower shoreface between 12 and 35 m water depths.

Figure 8 compares surveyed and equilibrium shoreface profiles from the same datasets and analyses for Warilla, Shellharbour North and Shellharbour South beaches (P5–P7), and the transect across the Bass Point shelf sand body (P8). Similar to P4, the Warilla Beach shoreface (P5) features a concave upper shoreface that transitions to a smooth convexity dominating the mid-lower shoreface, and a slightly concave lower shoreface-inner shelf. The Shellharbour North Beach and Shellharbour South Beach shorefaces have regular concave geometry, despite the proximity of P6 and P7 to mapped reef outcrops (Fig. 6c), and the discontinuous sediment distribution across the lower shoreface-inner shelf along P6 (Fig. 5b). The Bass Point shoreface is comparatively steep, falling almost vertically from the submerged reef platform extending from the rocky shore onto the headland-attached shelf sand body about 25 m below. The shelf sand body has typically convex geometry (Field and Roy 1984; Ferland 1990) and falls away steeply to the adjacent shelf seaward from about 40 m water depth.

The DN91 profile approximates the gradient and curvature of the surf zone (to 4 m water depth) at each profile, which reduces in seaward extent with decreasing wave exposure from north (P1) to south (P7) but predicts much shallower shoreface-inner shelf profiles than our high-resolution surveys (Figs. 7 and 8). The OA16 profiles provide a better fit of the upper to mid-shoreface geometry of all profiles relative to the DN91 profile. Only profiles P1, P6 and P7 have geometry approximately consistent with the OA16 profiles across the lower shoreface (i.e. between z_c and z_s). Profiles P2, P3, P4 and P5 deviate from the theoretical equilibrium geometry to varying degrees, while P8 is typical of a different geomorphic

Fig. 7 Shoreface depth profiles at **a** P1, **b** P2, **c** P3 and **d** P4 (Fig. 5) based on navigation bathymetry and our high-resolution bathymetry model. DN91 and OA16 theoretical equilibrium profiles calculated at P1–P4 are shown with the local upper (z_c), active (z_a) and lower (z_*) shoreface limits (Table 2). The OA16 profiles have been translated seawards such the their origins align horizontally with the breakpoint bar position (x_b) and are truncated above z_b for clarity



setting (headland-attached shelf sand body). We found that the OA16 profiles did not reflect the surveyed shoreface profiles with the origins aligned with the DN91 profiles (i.e. 2-m AHD elevation contour). This is not surprising as the OA16 profiles are based on shoaling wave processes and thus the equilibrium slopes are not applicable within the surf zone. We translated the OA16 profiles horizontally seawards such that their origins aligned with the breakpoint bar (z_b) on each surveyed profile (Figs. 7 and 8). The DN91 profile was not translated as it is based on empirical observations of surf zone profiles. The DN91 profile is not representative of shoreface geometry beyond the surf zone in our setting.

Active Zone

Applying Hallermeier's (1981) formula for d_i using wave climate statistics from the long-term Port Kembla wave buoy (Fig. 1b) record, we calculate a regional upper shoreface (inner

shoal zone) limit (z_c) of 10.9 m for fully exposed beaches. Similarly, following Hallermeier's (1981) formula for d_i using the same wave climate statistics and a representative shoreface sediment grain size of 250 μm , we calculate a regional lower shoreface (outer shoal zone) limit (z_*) of 30.8 m for exposed beaches with a shoreface of fine-medium sand. Table 2 compares the local z_c and z_* values calculated for each beach using local wave height scaling (c_H) and sampled sediment grain size (D_{50}). As Hallermeier's d_i varies only with the wave climate, the local z_c decreases with increasing attenuation of wave height moving north to south from Perkins Beach to Shellharbour South Beach. Because d_i is also sensitive to sediment grain size, the influence of reduced exposure to waves at Warilla Beach is offset by the finer shoreface sand, resulting in a slightly deeper local z_* than the more exposed Perkins Beach. Similarly, the fully exposed Bass Point shoreface has the deepest z_c value, although the coarser sand associated with the shelf sand body results in a moderate z_* value.

Fig. 8 Shoreface depth profiles at **a** P5, **b** P6, **c** P7 and **d** P8 (Fig. 5) based on navigation bathymetry and our high-resolution bathymetry model. DN91 and OA16 theoretical equilibrium profiles calculated at P5–P8 are shown with the local upper (z_c), active (z_a) and lower (z_*) shoreface limits (Table 2). The OA16 profiles have been translated seawards such the their origins align horizontally with the breakpoint bar position (x_b) and are truncated above z_b for clarity

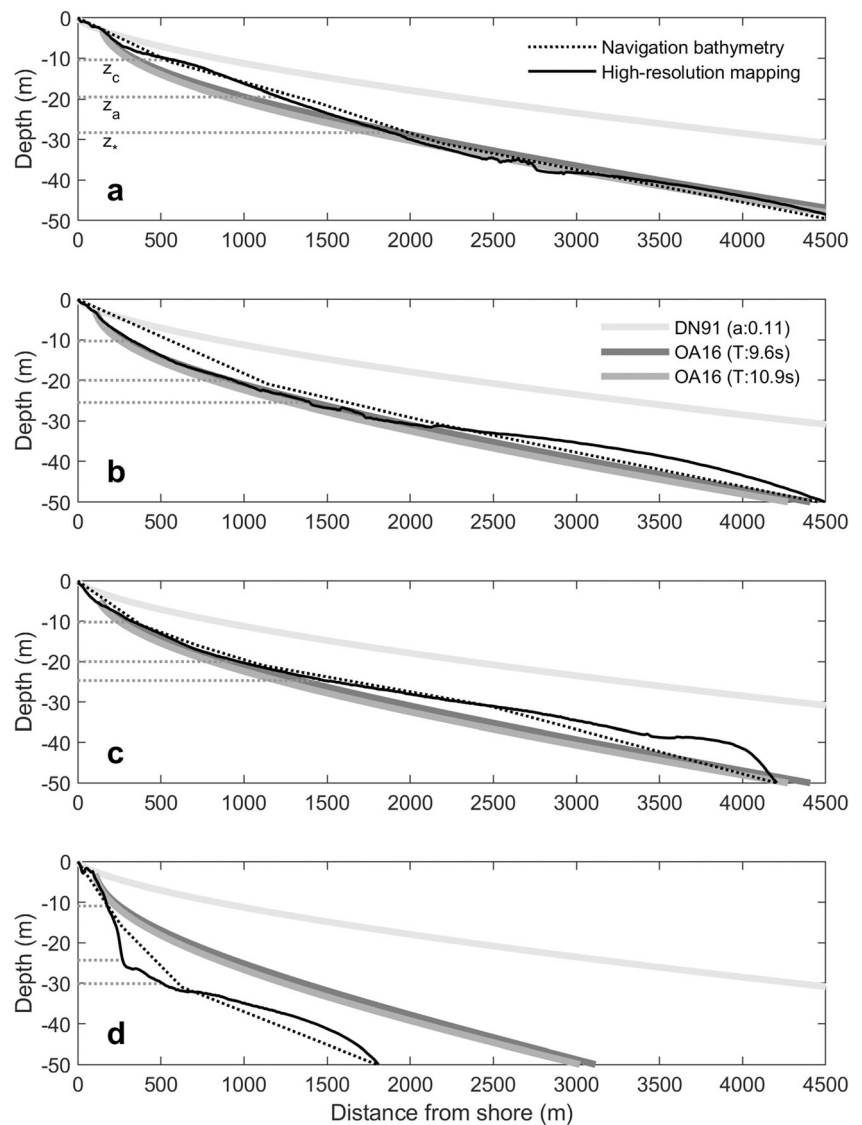


Table 2 Local and regional (Illawarra) values of upper shoreface (z_c) and lower shoreface (z_*) depth limits based on Hallermeier’s (1981) inner (d_i) and outer (d_o) shoal zone limits respectively, and active shoreface depth limits (z_a) based on Ortiz and Ashton’s (2016) morphodynamic depth of closure (MDOC) method for a 100-year timescale

	c_H (%)	z_c (d_i) (m)	D_{50} (μm)	z_* (d_i) (m)	w_s (m/s)	H_{30} (W1) (m)	z_a (W1) (m)	H_{30} (W2) (m)	z_a (W2) (m)
Perkins	92	-10.6	266	-27.1	0.031	2.7	20.4	3.3	25.1
Windang	89	-10.5	266*	-26.1	0.031*	2.6	20.0	3.2	24.6
Warilla	85	-10.4	203	-28.3	0.025	2.5	19.5	3.1	24.2
Shellharbour N	82	-10.3	229*	-25.5	0.028*	2.6	20.0	3.1	24.2
Shellharbour S	80	-10.2	229	-24.7	0.028	2.6	20.0	3.2	24.6
Bass Point	100	-10.9	321 [#]	-27.1	0.040	3.0	21.6	3.7	26.8
Illawarra	100	-10.9	250	-30.8	0.030	3.7 [^]	24.3	4.4 [^]	29.5

Local z_c and z_* values vary with relative exposure to the regional wave climate (c_H) and median sediment grain size (D_{50}) in 20 m water depth. Local z_a values are based on sediment fall velocity (w_s) for samples from 20 m water depth and morphodynamic wave height in 30 m water depth (H_{30}) with wave climate weightings of H^5 (W1) and $H^5 T^{-5} \sin^{-5}(kz)$ (W2) applied

*Sediment grain size from adjacent shoreface assumed in the absence of a grab sample from 20 m water depth

[#] The shallowest sediment sample retrieved from the Bass Point shelf sand body was in 33 m water depth

[^]Regional deep-water morphodynamic wave height (H_0) used

Applying Ortiz and Ashton's (2016) methods to calculate the MDOC for a timescale of 100 years, we calculate a regional active shoreface limit (z_a) of 24.3 m for W1 wave climate weighting and z_a of 29.5 m for W2 weighting. However, the regional values were calculated using deep-water wave height (H_0), and thus, we assume no wave height attenuation between deep water (z_w) and z_* , which is unrealistic for the embayed setting. Table 2 shows local z_a values calculated using H_{30} as determined by scaling the transformed wave climate (7-year record) in 30 m water depth off each beach to the deep-water morphodynamic wave climate based on the 45-year Port Kembla record (see the [supplementary material](#)). Our z_a values scale with H_{30} as the MDOC is, perhaps surprisingly, insensitive to sediment grain size (Ortiz and Ashton 2016). The regional and local z_a values based on W2 weighting are about 5 m deeper than the values based on W1 weighting. Notably, the z_a values calculated for a 100-year timescale fall between the z_c and z_* values calculated using Hallermeier's formulae, and the W2 weighted values approach z_* . Our results therefore suggest that in this setting, most of the shoreface (extending to Hallermeier's d_i) may be morphodynamically active over a 100-year timescale.

Shoreline Change Analysis

Historical

The Perkins-Windang shoreline has experienced a mild clockwise rotation during the past four decades, with Perkins Beach accreting and Windang Beach receding, except near the Lake Illawarra entrance (Fig. 2a). We truncated our photogrammetry analysis at 2014 to evaluate if that signal is related to a severe coastal storm in 2016, which impacted central to southern ends of NSW beaches (Harley et al. 2017). The result was similar, however, reflecting a previous study that identified the clockwise rotational trend (Cardno 2010). Doyle et al. (2019b) found that Perkins-Windang Beach accreted by around 120 m³/m of shoreline on average during 1961–2014. The construction of the Lake Illawarra entrance training walls (2001–2007) triggered scouring of sand shoals and channels within the tidal inlet, which appears to be driving progradation of the flood-tidal delta into the lake and aggradation of the ebb tidal delta outside the entrance, while increasing the tidal range within the lake (Young et al. 2014; Wiecek et al. 2016; Hart et al. 2017). Although the long-term average trend found by Doyle et al. (2019b) is likely influenced by human interventions, the beach is located on a prograded-stationary barrier and thus the Perkins-Windang shoreline is considered stable.

The southern half of Warilla Beach appears to be stable to slightly accreting while the northern half shows a strong accretionary trend related to the construction of the inlet training walls in 2001–2007 and active stabilisation of the northern

end of the beach (Fig. 2b). This is consistent with Doyle et al. (2019a) who found that after the loss of about 400 m³/m of dune volume due to human activities in the 1950s and 1960s, the dune was stabilised and has grown gradually to the present day. Doyle et al. (2019a) documented human interventions that influenced the historical record of beach behaviour, including removal of the natural dune vegetation (1930s), mining of the northern dune for sand (1940s), levelling of the southern dune for housing development (1960s), construction of a rock wall in the southern dune and a groyne at Little Lake inlet to protect housing (1970s), dune stabilisation and revegetation (1980s) and stabilisation of the Lake Illawarra entrance through construction of the southern (2001) and northern (2007) training walls, during which sand dredged from the tidal inlet was pumped onto Warilla Beach. Typical of this setting, the beach and foredune experience periodic fluctuating erosion caused by storms and wave climate variability (Clarke and Eliot 1988) and were heavily impacted by severe storms in the 1970s and in 2016 (Harley et al. 2017).

Shellharbour North Beach is stable historically and shows a slight accretionary trend along the entire beach (Fig. 2b). Shellharbour South Beach shows a much stronger accretionary trend (Fig. 2b), which is thought to reflect recovery following the impact of a severe storm (most likely May 1997), during which the low foredune of this usually sheltered beach was apparently overwashed and removed (SMEC 2010). The gap in our analysis along the southern half of Shellharbour South Beach marks the site of an artificial harbour entrance that is under construction. Our findings reflect SMEC (2010) who also found that both beaches have accreted historically, and Shellharbour South at a faster rate.

Future

The potential importance of shoreface morphodynamic activity to future shoreline response (assuming the Bruun effect) due to a 1-m sea level rise was investigated by applying the Bruun Rule using local values of z_c , z_a (W1 weighting) and z_* (Table 2) for closure depth. Table 3 shows the predicted shoreline retreat at each profile for the three closure depths. Values are provided for profiles derived from navigation bathymetry (Fig. 1b) and from our high-resolution bathymetry model (Fig. 5a). The comparison shows that shoreline retreat predicted by the Bruun Rule using the active shoreface limit (z_a) as closure depth is usually, but not always between the shoreline retreat distances predicted when using the upper (z_c) and lower (z_*) shoreface limits as closure depth. That is to be expected for regular concave profile geometry, and departures thus indicate irregular profile geometry. Shoreline retreat predicted by the Bruun Rule using shoreface profiles derived from high-resolution mapping was less than that predicted for profiles derived from navigation bathymetry by between 5 and 17 m

Table 3 Shoreline change (m) in response to a 1-m sea level rise predicted by the profile approach using the Bruun Rule and measured landward from the foredune crest at profiles P1–P7

Beach	Profile	Dune crest (m)	Navigation bathymetry			High-resolution mapping		
			z_c	z_a	z_*	z_c	z_a	z_*
Perkins	P1	6.5	38	55	57	30	44	52
	P2	6.5	30	54	61	26	40	54
Windang	P3	7.5	28	49	63	24	49	69
	P4	5.5	43	64	65	29	61	62
Warilla	P5	6.5	44	57	60	39	49	56
Shellharbour N	P6	4.4	46	51	62	28	42	50
Shellharbour S	P7	4.2	33	50	57	30	44	55

Predictions for shoreface profiles derived from navigation bathymetry (Fig. 1b) and our high-resolution bathymetry model (Fig. 5a) are provided for local closure depths (Table 2) of z_c , z_a (W1) and z_*

when using z_a as closure depth. Modest differences reflect profiles where existing navigation bathymetry compares reasonably well with the high-resolution mapping, in the vicinity of the closure depth, whereas larger differences indicate areas where the navigation bathymetry provides a poorer representation of the shoreface morphology (Figs. 7 and 8). We compare these findings with predictions based on a compartment approach to shoreline change analysis later in the discussion.

Discussion

Geomorphology and Sediment Distribution

Compartment Classification

One third of the compartment is formed of low-profile rocky reefs, which are more extensive than what was previously known (Fig. 6c). The seabed is sediment dominated nonetheless—e.g. 60% of the adjacent Wollongong compartment seabed is reef platforms (Linklater et al. 2019). The prominence of Red Point and the extensive reef platform extending offshore to the limit of our survey and north to Five Islands suggest that the northern compartment boundary is probably closed to significant alongshore sediment transport at intermediate timescales (Fig. 5a). Fringing reefs extend from rocky shores around all headlands (including Windang Island) into 15–30 m water depths, such that the sandy mid-lower shorefaces off Warilla, Shellharbour North and Shellharbour South beaches are much narrower than the respective shoreline lengths (Fig. 6d). Despite that, cross-shelf sediment transport pathways connect all five beaches to the inner shelf indicating the potential for shoreface sediment sources and sinks to influence shoreline behaviour. Aside from these fringing reefs, reef platforms occur deeper on the inner shelf mostly beyond the lower shoreface limit (z_*). The rocky reefs form part of the East Australian marine abrasion surface, which is a planar bedrock surface that

is variably exposed for some 300 km north and south of Sydney along the inner- to mid-continental shelf of central NSW (Thom et al. 2010). It is thought to be the product of long-term wave erosion of antecedent coastal cliffs that have retreated about 20 km over the past 30 million years to the present coastline as the continental margin slowly subsided.

We divide Perkins and Windang beaches into two sub-compartments reflecting contrasting shoreface geomorphology and morphodynamics as discussed further below. The sub-compartment boundary is open as there is no impediment to alongshore littoral sand transport. Mid-shoreface irregular scour depressions occur throughout the Windang sub-compartment but are absent from Perkins (Fig. 5a). Although Windang Island appears to be a prominent headland, it is connected by a narrow sandy tombolo to both the southern end of Windang Beach (south of the Lake Illawarra entrance) and the northern end of Warilla Beach (Fig. 2b). Lake Illawarra is known to have periodically opened onto Windang and Warilla beaches prior to entrance training in 2001–2007 (Doyle et al. 2019a), and intermittent sediment bypassing across the low tombolo is possible today. We consider Windang Island and its tombolo to be a leaky tertiary compartment boundary under modern conditions (Fig. 5a). The Shellharbour North and Shellharbour South tertiary compartments are essentially closed under present conditions. The deeply embayed locations relative to Bass Point and the refraction of waves from the south-southeast suggest that sediment sharing is absent or negligible between those beaches. The shorefaces are separated by a prominent rocky reef platform that extends into 30 m water depth around Shellharbour. While both tertiary compartments have near-equilibrium shoreface geometry (Fig. 8), the Shellharbour North inner shelf has a disrupted sediment distribution, whereas shoreface sand grades to fine inner-shelf sand off Shellharbour South Beach (Fig. 5b).

The profile off Bass Point (Fig. 8d) shows that the top of the shelf sand body lies below the OA16 equilibrium profiles

and also the lower shoreface limit (z_*), and is therefore unlikely to provide a pathway for headland sand bypassing (e.g. Goodwin et al. 2013) from the Kiama compartment to the south. The sand body has a maximum thickness of 21 m to the underlying bedrock and is relatively small compared to others in the region (Ferland 1990). Shelf sand bodies are thought to be reworked remains of transgressive barriers that became stranded on steeper sectors of the inner shelf (usually off headlands and coastal cliffs) when sea level flooded highstand embayments towards the end of the Holocene post-glacial transgression (Ferland 1990; Roy et al. 1994; Roy 2006). Narrow channels of very coarse and shelly sand that we mapped and sampled on the Bass Point shelf sand body (Figs. 5b and 6d) were also observed by Field and Roy (1984) on shelf sand bodies off the Sydney coast and interpreted as scour channels indicating downwelling bottom currents and offshore-directed sediment transport. Both the profile off Bass Point (Fig. 8d) and the evidence of offshore transport suggest that the southern compartment boundary is closed at intermediate timescales.

Shoreface and Inner-Shelf Sand

The sediment types and their distributions reflect existing depth-based shelf sedimentation models for this coast (Roy and Stephens 1980; Roy and Thom 1981; Roy 2006), although the abundance of rocky reefs impart additional complexity (Fig. 6d) and carbonate content varies markedly at a local scale (Fig. 5b). Shoreface sand comprises reworked (rounded grains) and moderately well-sorted medium to fine quartz grains (some iron stained) with lesser carbonate, lithic and feldspar grains. Decreasing grain size from medium to fine sand from the upper to lower shoreface is consistent with Roy and Stephens' (1980) medium-coarse inner nearshore sand (from the beach to 5–12 m water depths) and fine outer nearshore sand (to 15–30 m water depths). Fine sand from the Lake Illawarra inlet opening onto Warilla Beach prior to entrance training likely contributed to the finer texture of upper shoreface sand there (Fig. 5b), and sand dredged from the inlet and used to nourish the beach (Doyle et al. 2019a) may have also leaked offshore (Thieler et al. 2001). The carbonate content of shoreface sand is locally variable, being low (< 10%) on the Perkins shoreface and moderate (20–35%) to high (> 50%) on shorefaces south of Windang Island. This pattern is generally consistent with carbonate contents of 6.9% for sand from Perkins Beach, 34.3%, 17.2% and 20.2% on Warilla, Shellharbour North and Shellharbour South beaches, and 60.4% within Shellharbour (Short 2020). The sandy shorefaces off the latter beaches are all flanked by rocky reefs surrounding the adjacent headlands. These fringing reef platforms occur in shoreface waters (< z_*) and appear to contribute a significant component to the sediment budget. In contrast, large reef platforms off Perkins-Windang Beach are

mostly beyond the shoreface (> z_*), and the shoreface and beach sand are low in carbonate content. Thus, carbonate content varies locally with the occurrence of rocky reefs that support carbonate organisms including molluscs, bryozoans and coralline algae, and the water depth and morphology of rocky reefs appear to be an important control on carbonate entering the beach-shoreface sediment budget.

The distinct coarse and fine inner shelf sand is most evident in the central compartment off Windang, Warilla and Shellharbour North beaches (Fig. 6d), where the shoreface sand transitions sharply to inner-shelf coarse sand. It is consistent with the inner-shelf sand sheet described by Roy (2006), which is a transgressive deposit extending from 20 to 35 m water depths to around 60 m water depth that was abandoned by landward migrating barriers during the Holocene post-glacial sea level rise. It features an irregular distribution of heavily reworked coarse (iron stained) and fine quartz sand that develops from wave-sorting of the same palimpsest parent material—i.e. the fine sand is the finer fraction that is periodically mobilised on top of the coarser fraction by waves and currents. The offshore boundary between the coarse and fine sand is abrupt and is marked by a prominent 0.5-m step up to the fine sand (Fig. 5). The step is anchored to reef outcrops and has an arcuate form that is consistent with the fine sand being organised by bottom currents. Exposure of coarse sand between 25 and 35–45 m water depths in the central compartment suggests that the lower shoreface-inner shelf is subject to erosional scouring there. This may be due to complex hydrodynamics enhanced by the abundant rocky reefs, as the lower shoreface geometry is not grossly dissimilar from Perkins or Shellharbour South (Figs. 7 and 8). The occurrence of mid-shoreface irregular scour depressions in the central compartment (Fig. 5a) also suggests complex bottom currents and limited shoreface sand cover (Thieler et al. 1995, 2001), perhaps due to rip current activity off those beaches (Short 2020).

The transition from shoreface to inner-shelf sand is less apparent off Perkins and Shellharbour South beaches where lower-shoreface fine sand grades indistinctly into inner-shelf fine sand around 40 m (sample 2) and 30 m (sample 30) water depths, respectively (Table 1). There is no abrupt change in grain size or carbonate content to distinguish facies boundaries (Fig. 6d). A shoaling gradient in the shoreward limit of inner-shelf fine sand from north to south, with reduced exposure to wave energy, is evident in both the alignment of the raised step that separates the coarse and fine inner-shelf sand in the central compartment (45 m water depth at Windang to 35 m at Shellharbour North) and the gradation from shoreface to inner-shelf fine sand off Perkins and Shellharbour South beaches. The transition (whether abrupt or gradual) to inner-shelf fine sand lies beyond our predicted z_* (Table 2) in all cases. This is not surprising, however, considering that Hallermeier's (1981) d_i identifies the seaward limit of

significant cross-shelf sediment transport at annual timescales, while the distribution of inner-shelf sand has evolved over much longer timescales (centuries to millennia). We compare our theoretical shoreface limits with depositional evidence later in the discussion. The mid-shelf fine sand (samples 1, 6 and 23) is distinguished by its grain size ($< 150 \mu\text{m}$), carbonate content ($> 20\%$), slightly cohesive character and colour (olive-grey). The transition to mid-shelf fine sand (Fig. 6d) marks the extent of shelf sediment that is relevant to the beach-shoreface sediment budget at long timescales (millennia).

Shoreface Morphodynamics

While the upper shoreface limit (z_c) can be measured through repeat seabed surveys carried out over yearly-decadal timescales (e.g. Nicholls et al. 1998), the transition from shoreface to inner shelf (z_*) and the extent of the active zone (z_a) may not be evident due to increasing morphological response timescales across the lower shoreface-inner shelf (Niedoroda et al. 1984; Stive and de Vriend 1995; Cowell and Kinsela 2018). Present-day morphology and sediment distributions may not reflect coastal evolution at the intermediate timescales (decades to centuries) of interest for coastal risk management and planning, instead capturing processes occurring over shorter (seasons to years) or longer (millennia) timescales. We compare the surveyed shoreface geometry and critical limiting depths (z_c , z_* and z_a) with depositional evidence to interpret shoreface morphodynamics.

Upper Shoreface

The concave upper-shoreface geometry found off all beaches (Figs. 7 and 8) reflects the energetic wave climate and sandy upper shoreface in our setting (Wright 1995; Short 2020). The surf zone profiles extend up to 300 m from shore, with the surf zone width decreasing with reduced exposure to wave energy moving south along the compartment shoreline. The surf zone profiles are consistent with the DN91 profile for medium sand. An inflection in 4–5 m water depths marks the toe of the surf zone at the breakpoint bar (z_b) and the transition to the broader upper shoreface profile. It also marks the transition from shoaling wave (upper shoreface) to breaking wave (surf zone) sediment transport processes for wave conditions at the time of the lidar survey. Upper-shoreface geometry beyond the surf zone (from z_b to z_c) is steeper and universally concave. The full upper shoreface profiles (z_0 to z_c) closely resemble the bar-berm and shorerise morphology described by Inman et al. (1993). They found that beach-nearshore profiles in Southern California could be described by two separate curves crossing at z_b , which marks the transition from bar-berm (surf zone) geometry to shorerise (upper shoreface) geometry. By fitting DN91 profiles to approximate the shorerise and bar-

berm profiles, they found that best-fit shorerise profiles passed through an origin at $z = 0$ while bar-berm profiles passed through a point 1.3 m above the berm crest, reflecting that the lower beach face is shaped by swash waves and is an extension of the surf zone profile geometry.

Our results show that shoreface profiles in our setting can be approximated using the DN91 profile for the surf zone (bar-berm) and the energetics-based OA16 equilibrium profile for the shoreface beyond z_b (shorerise). This suggests that where the shoreface geometry approaches equilibrium in our setting, it can be predicted from wave climate and sediment data alone. That is the case across the upper shoreface for profiles P1, P2 and P3 (Fig. 7), and P6 and P7 (Fig. 8), and also across the lower shoreface where sedimentary shorefaces are distal from reef structures or sediment lobes (P1, P6, P7). The upper shoreface is therefore in a graded (near-equilibrium) morphodynamic state at all profiles, except P4 (Fig. 7d), P5 (Fig. 8a) and the Bass Point shelf sand body (Fig. 8d). The profile convexities off Windang (P4) and Warilla (P5) beaches are indicative of overfit profiles and provide opportunities to assess our predicted z_c values, because wave processes should maintain statistically stationary profile geometry across the upper shoreface over an annual timescale (Hallermeier 1981; Nicholls et al. 1998). Inspecting the shoreface geometry at P4 and P5, concave geometry extends out to 10–12 m water depths, or about our local z_c based on Hallermeier's (1981) inner shoal zone limit (Table 2), although profile geometry remains overfit relative to the equilibrium geometry predicted by the OA16 profiles. This suggests that sediment accommodation could be generated by sea level rise across the upper shoreface at P1, P2, P3, P6 and P7, while the overfit shorefaces at P4 and P5 might limit upper-shoreface response to sea level rise there.

Lower Shoreface and Active Zone

Concave profile geometry extends across the lower shoreface (to z_*) where the sedimentary profile is not otherwise influenced by reef structures or sediment lobes (e.g. P1, P6, P7). The Perkins Beach shoreface geometry is close to equilibrium, suggesting potential for shoreface response to sea level rise beyond the upper shoreface. Profile P1 (Fig. 7a) shows relatively linear shoreface geometry, while P2 has a lower shoreface-inner shelf convexity between 28 and 45 m water depths (Fig. 7b). The convexity is smooth and is distal from adjacent rocky reefs but occurs in deeper water than the P4 (Fig. 7d) and P5 (Fig. 8a) profile convexities. The P2 convexity provides an opportunity to assess our theoretical prediction of z_* . The upper surface of the convexity in 28 m water depth lies within 100 m from our calculated local z_* of 27.1 m (Table 2) as it is planar where it meets with the concave shoreface profile above (Fig. 7b). This suggests that the upper surface of the convexity is erosional, consistent with the lower shoreface eroding into an inherited shoreface sand body. Our

findings suggest that the entire shoreface-inner shelf at P1 is in a near-equilibrium morphodynamic state, whereas the P2 shoreface is to about z_a , with the lower shoreface-inner shelf beyond being overfit. The divergence between observed and equilibrium shoreface geometry around z_a at P2 is notable as it suggests that the lower shoreface may provide a subtle ongoing sand supply to Perkins Beach that might promote shoreline stability and potentially offset shoreline response to sea level rise.

Sand supply from the lower shoreface to Perkins Beach is consistent with the long-term historical accretion of that shoreline (Doyle et al. 2019b) and could represent a remnant process of shoreface lowering due to morphodynamic disequilibrium-stress, which would explain initial progradation of the Holocene Perkins-Windang barrier. That process has been shown to be the primary source of Holocene barrier progradation elsewhere in southeastern Australia (Kinsela et al. 2016). While the inner-shelf profiles (beyond z_*) at Shellharbour North (Fig. 8b) and Shellharbour South (Fig. 8c) beaches are also shallower than the equilibrium geometry, the discontinuous sediment distribution of the former and the sheltered setting of the latter suggest that a shoreface sand supply is unlikely to be active or significant. This is consistent with stationary barrier development, which reflects more limited sediment supply (Roy et al. 1994). The graded (near-equilibrium) profile geometry above z_* does, however, suggest the potential for sea level rise to generate sediment accommodation across the lower shoreface at Shellharbour North and Shellharbour South beaches, which might extend to z_a over intermediate timescales (decades to centuries).

The Windang and Warilla shoreface profiles vary from the concave geometry found elsewhere. At Windang Beach, profile P3 is truncated above z_* by a large rocky reef platform (Fig. 7c). Further south, the smooth shape of profile convexities and continuous sediment cover suggests that the geometry of the mid-lower shoreface profiles off Windang and Warilla beaches is influenced by sediment lobes along P4 (Fig. 7d) and P5 (Fig. 8a), respectively. The convexity begins in 10–12 m water depths (just beyond z_c) on both profiles, and concave profile geometry is resumed in 20–25 m water depths. The proximity of P4 and P5 to the Lake Illawarra entrance, and historical accounts of entrance opening onto both beaches prior to the construction of training walls between 2001 and 2007 (Doyle et al. 2019a), indicates that the convex features may be ebb-delta sand bodies. The geomorphic evidence implies that the lower shorefaces at Windang Beach (south of P3) and at Warilla Beach are presently in overfit morphodynamic states (negative sediment-accommodation), meaning that any potential generation of sediment accommodation and shoreface response to sea level rise may be limited to z_c . As the upper shorefaces at P4 and P5 also appear to be overfit, any initial response to gradually rising sea level could be partially offset by shoreface supply, although the alongshore extents of the sand bodies are much less than the adjacent shorelines.

The separation of shoreface sand from fine inner-shelf sand off Windang, Warilla and Shellharbour North beaches (Fig. 6d) provides further evidence to evaluate local z_* values. Notably, the z_* value of 28.3 m water depth for Warilla Beach closely reflects the offshore extent of fine lower shoreface sand at P5, which transitions to coarse inner-shelf sand in 28–29 m water depths (Fig. 5b). Similarly, the z_* value of 25.5 m for the shoreface off Shellharbour North Beach is consistent with the extent of fine lower shoreface sand at P6, which transitions to coarse inner-shelf sand between 25 and 26 m water depths. Inspection of grab sample 19, which was retrieved from an isolated patch of fine sand in 27 m water depth (Fig. 5b), reveals that sand to be more comparable to fine inner-shelf sand (samples 21, 22 and 23) than the fine lower shoreface sand (samples 3, 13 and 31) that is found in similar water depths off Perkins, Warilla and Shellharbour South beaches (Table 1). Although the transition from shoreface sand to coarse inner-shelf sand is less clear in the backscatter data off Windang Beach, the character of grab sample 11 and the backscatter signal in that vicinity (Fig. 5b) suggests that the transition is also consistent with a z_* value of –26.1 m there. The transition from shoreface sand to inner-shelf coarse sand only has a morphological expression (similar to the 0.5-m step between the coarse and fine inner-shelf sand) at Shellharbour North Beach (Fig. 5a). The consistency between the seaward extent of shoreface sand where it is evident in the central compartment and z_* values based on Hallermeier's (1981) formula is compelling because it suggests that the annual limit of significant cross-shelf sediment transport (d_i) is a meaningful limit for the cross-shelf sediment budget at intermediate timescales.

It is notable that proximity to rocky reefs does not seem to be a predictor of bedrock influence on shoreface geometry in our setting. The profiles off Shellharbour North (Fig. 8b) and Shellharbour South (Fig. 8c) beaches have geometry consistent with the OA16 equilibrium profiles despite being the narrowest sandy shorefaces in the compartment and flanked by rocky reef (Fig. 6d). This reflects the low-profile and planed relief of rocky reef platforms associated with the East Australian marine abrasion surface (Thom et al. 2010) and implies that proximity to reefs is not a reliable indicator of the geometry and morphodynamic state of the shoreface in this setting. That relationship is unlikely to extend to the sediment thickness, however, as the nearshore sediment volume is likely to decrease with proximity to local exposures of underlying stratum (Miselis and McNinch 2006). Conversely, the observed profile geometry is also not a reliable indicator of the shoreface-inner shelf sediment distribution. While both P6 and P7 have near-equilibrium profile geometry, the distribution of fine sand across the Shellharbour North shoreface-inner shelf is discontinuous, whereas shoreface sand grades continuously into inner-shelf fine sand off Shellharbour South Beach (Fig. 6d). The results highlight the importance of

detailed shallow-water seabed mapping and sampling in our setting to characterise shoreface geomorphology and morphodynamics for sediment budgeting.

There is limited morphological or sedimentary evidence to support or refute our active zone limits (z_a) calculated using the MDOC method (Ortiz and Ashton 2016). This is not surprising as z_a is a timescale-dependent limit and the values provided in Table 2 were derived for an arbitrary timescale of 100 years (z_{a100}) in the context of gradual and depth-dependent wave-driven sediment transport processes that control shoreface-inner shelf geometry and sediment distributions. These values are nonetheless useful for considering the extent of the shoreface that maybe morphodynamically active at intermediate timescales, and thus, the potential dimensions of the shoreface sink for sediment budgeting and shoreline change prediction. Notably, our z_{a100} values calculated using the MDOC method fall between the z_c and z_* values calculated using Hallermeier's (1981) inner and outer shoal zone limits (Table 2), which supports a prior investigation of shoreface morphological response timescales (Cowell and Kinsela 2018). The shoreward limit of our MBES surveys was about 20 m water depth, around our z_{a100} values based on W1 weighting. Thus, the transition from MBES data to lidar data hinders rigorous evaluation of evidence for z_a in the bathymetry and intensity data. Inspection of the lidar reflectivity data and the backscatter data at the lidar-MBES interface revealed no obvious discontinuities, aside from a slight change in shoreface slope at Shellharbour North Beach that is evident in profile P6 becoming steeper beyond 20 m water depth (Fig. 8b). Our z_{a100} values based on W2 weighting approach the z_* values calculated using Hallermeier's (1981) outer shoal zone limit (Table 2), suggesting that the entire shoreface may be morphodynamically active over a 100-year timescale. Empirical observations from the Gold Coast (Fig. 1a) suggest that z_{a100} might be slightly less than 20 m water depth there (Patterson and Nielsen 2016), although varying shelf setting and predominantly cross-shelf transport processes on our embayed coast make direct comparison difficult. A theoretical z_{a100} derived using the MDOC method should extend beyond shoreface adjustment detectable in a multi-decade seabed survey dataset, and broad agreement is therefore encouraging.

Shoreline Change Analysis

Our application of the Bruun Rule to predict shoreline change due to sea level rise using representative beach-shoreface profiles (P1–P7) followed the standard approach often applied in practice. It has many limitations in the Illawarra South compartment, where our mapping reveals a complex mixed sediment and rocky reef shoreface and alongshore variation in shoreface geometry. It is erroneous to suppose that shoreface response to sea level rise following the Bruun effect could be realised throughout an embayment where large reef structures truncate the shoreface, thereby limiting the potential shoreface accommodation-volume generated by sea level rise. Where

they are continuous alongshore, reefs might directly control the location of z_c , z_a and/or z_* (a perched beach-shoreface system), and where discontinuous, they at the least impose a negative sediment-accommodation volume proportionate to their surface area, thus restricting the potential sediment demand relative to the shoreline length along which it is distributed. Similarly, where the profile geometry of a sedimentary shoreface varies alongshore, it cannot be presumed that one sector of continuous sandy shoreline might respond differently to an adjacent sector due to local manifestation of the Bruun effect. Littoral sediment transport processes would distribute any sediment loss along the shoreline. These conditions violate basic assumptions of the Bruun Rule (Bruun 1983, 1988), and thus, the shoreline change predictions in Table 3 are inherently flawed, regardless of whether they are based on navigation bathymetry or high-resolution mapping data.

Compartment Approach

We can apply some simple compartment assumptions to investigate the implications of alongshore variation in shoreface geometry and a mixed sediment-reef substrate for modelling the shoreline response implied by the Bruun effect within the Perkins-Windang tertiary compartment (Fig. 5a). Like the profile approach described above, we apply the standard Bruun Rule with a 1-m sea level rise to simulate cross-shore sediment exchanges implied by the Bruun effect. In the compartment approach, however, we use alongshore averaging to capture the alongshore variation in shoreface geomorphology (Cowell et al. 2003a). We derive three alongshore-averaged profiles for comparison (Fig. 9): (1) Perkins-Windang tertiary compartment shoreface, (2) the same Perkins-Windang shoreface excluding mapped reefs and (3) Perkins sub-compartment shoreface excluding mapped reefs (Fig. 6c). We averaged high-resolution shoreface bathymetry (with mapped reefs included or omitted) in ArcGIS 10.4 along shore-parallel contours spaced 20 m across the shoreface, beginning from a smoothed 2-m AHD elevation contour that reflects the shoreline orientation and beach berm position (Fig. 6c). The Perkins sub-compartment profile (no reefs) has concave lower shoreface geometry that is consistent with the fitted (least-squares regression) equilibrium function $z = -0.325x^{0.593}$, and is presumed to have a graded morphodynamic state (Fig. 9). In contrast, the Perkins-Windang tertiary compartment profiles are influenced by the shoreface reef platform at P3 (Fig. 7c) and the ebb-delta sediment lobe at P4 (Fig. 7d), and lower shoreface geometry is consequently overfit (Fig. 9). We therefore assume that upper shoreface response to sea level rise (to z_c) is possible throughout the Perkins-Windang tertiary compartment and apply the Bruun Rule using the Perkins-Windang (no reef) average profile with closure depth (z_c). As lower shoreface response (to z_a or z_*) is restricted to the Perkins sub-compartment, however, we apply

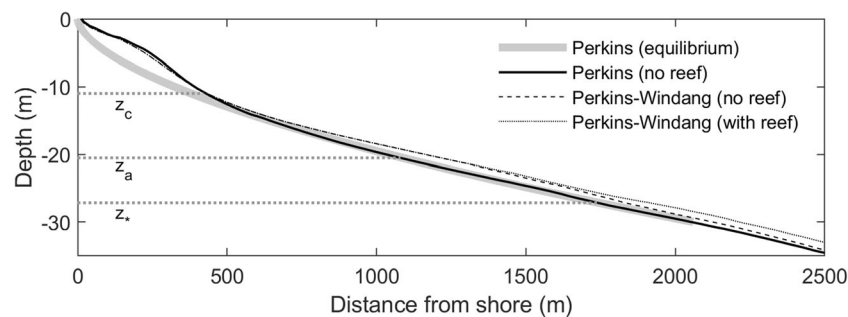


Fig. 9 Alongshore-averaged shoreface depth profiles derived from our high-resolution bathymetry model (Fig. 6c), including or excluding mapped reef outcrops as indicated, for the Perkins sub-compartment

the Bruun Rule again using the Perkins (no reef) average profile with closure depths of z_a and z_* . We scale the shoreline change predictions for the upper (Perkins-Windang) and lower (Perkins only) shoreface responses by the shoreface area within the Windang (45%) and Perkins (55%) sub-compartments, respectively, and distribute the combined sediment loss along the full length of the Perkins-Windang tertiary compartment shoreline (6.8 km) applying an alongshore-averaged foredune crest height.

Figure 10 compares shoreline change predictions based on the profile and compartment approaches at P1–P4 and demonstrates the sensitivity of the profile approach to alongshore variation in shoreface geometry. The lidar-derived beach-dune profiles are aligned at the baselines (dashed red) for our shoreline change predictions, which accommodate the impact of a severe erosion event. That is, the profile seaward (right) of the foredune crest position is the beach fluctuation zone, which has a volume that scales with shoreline exposure to waves ($210 \text{ m}^3/\text{m}$ at P1, $190 \text{ m}^3/\text{m}$ at P2 and P3 and $170 \text{ m}^3/\text{m}$ at P4). The shoreline change predicted by the profile approach varies between P1 and P4 with alongshore variation in shoreface and dune morphology, while shoreline change predicted by the compartment approach remains consistent between profiles. That is because the sediment exchange implied by the Bruun effect is calculated for compartment-average shoreface and dune morphology and is distributed along the beach. Shoreline change predictions for a closure depth of z_c are relatively similar between the profile and compartment approaches at P1–P4, reflecting that the upper shoreface geometry is relatively consistent along Perkins-Windang Beach (Fig. 7). For a closure depth of z_a , the predictions are 4–8 m less for the compartment approach at P1–P3 and 25 m less at P4, while for a closure depth of z_* predictions are 10–12 m less at P1 and P2, 27 m less at P3 and 20 m less at P4. Deviation between predictions from the profile and compartment approach reflects the sensitivity of the former to local variations in shoreface geometry, and the consideration of a mixed sediment-reef substrate in the latter. The profile approach implies that shoreline response to a 1-m sea level rise would vary by 20–30 m along the continuous Perkins-Windang Beach due to local variation in cross-shore sediment exchange. The reduced

and the Perkins-Windang tertiary compartment. The equilibrium profile fitted to the Perkins (no reef) profile is shown with the local upper (z_c), active (z_a) and lower (z_*) shoreface limits for Perkins Beach (Table 2)

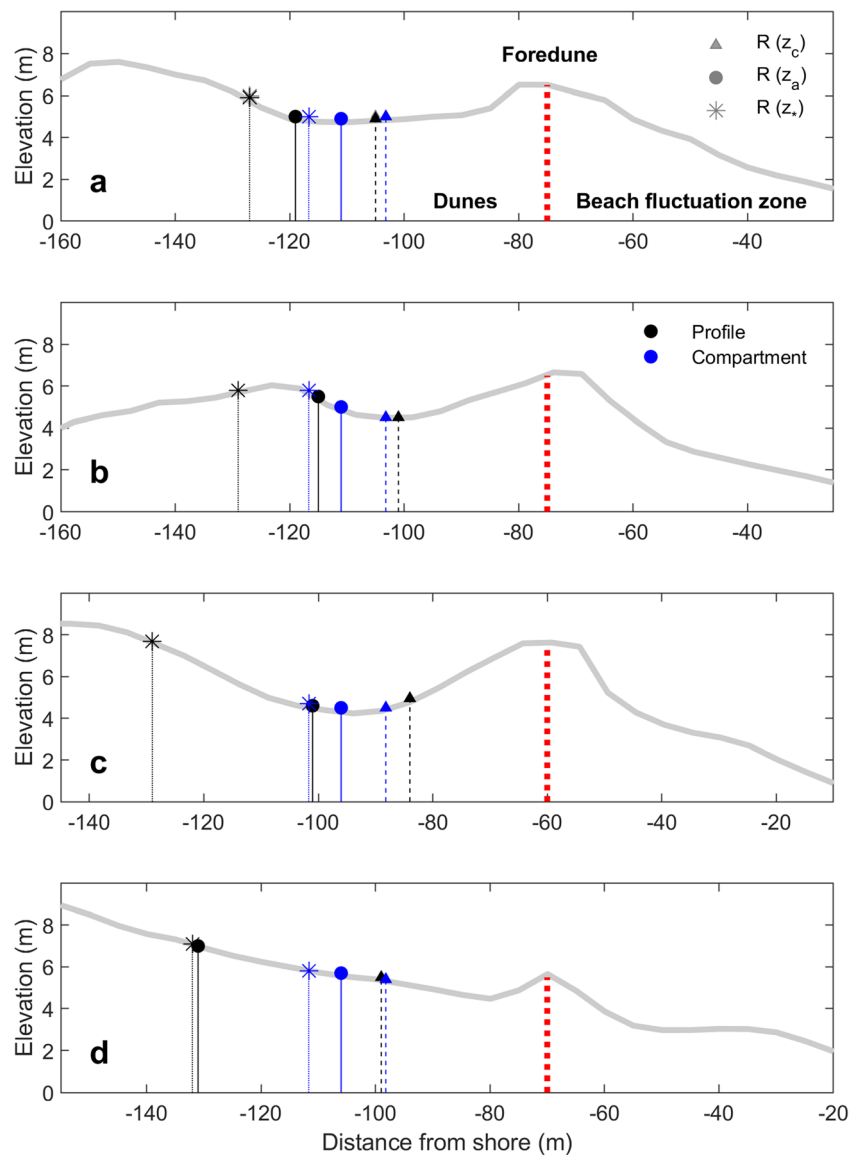
shoreline change predicted by the compartment approach follows our analysis of shoreface morphodynamics, which found that only within the Perkins sub-compartment is the lower shoreface a *potential* sediment sink for a 1-m sea level rise.

Towards Compartment Sediment Budgets

Our simple example of applying compartment thinking to consider shoreface response to sea level rise offers a rudimentary demonstration of the potential importance to shoreline change modelling (Fig. 10). Our example was limited to the sediment exchange implications of the Bruun effect (as expressed by the Bruun Rule) and ignored other important sediment budget components. Thus, our modelling should not be considered beyond that context. Other influences on shoreline response to sea level rise in our setting include the ongoing response of the Lake Illawarra flood-tidal delta to entrance training (Young et al. 2014; Wiecek et al. 2016; Hart et al. 2017) and potential sediment sequestration from the Windang shoreface to maintain dynamic equilibrium morphology with rising sea level (Van Goor et al. 2003). We also ignored the potential for ongoing shoreface sand supply from the lower shoreface sand body at Perkins Beach (Fig. 7b). Sub-surface imaging and coring of the shoreface-inner shelf sediment could provide important evidence to improve our assessment of shoreface morphodynamics and shoreline change (Miselis and McNinch 2006; Schwab et al. 2013). Another factor to consider given our sedimentology results is the impacts of ocean acidification on the carbonate sediment budget, particularly for beaches south of Windang Island. Simeone et al. (2018) predicted around a 30% loss in carbonate sediment on Mediterranean mixed carbonate beaches due to decreased production and increased dissolution for current projections of ocean acidification this century. A comparable loss of carbonate sediment from the Illawarra South compartment could have a significant influence on shoreline change over intermediate timescales. We recommend further research into all of these sediment budget components in this setting.

Our methods nonetheless offer a means to improve prior assessments of future shoreline change in southeast Australia. Kinsela et al. (2017) carried out a second-pass assessment of

Fig. 10 Predicted shoreline change (R) in response to a 1-m sea level rise at **a** P1, **b** P2, **c** P3 and **d** P4 (Fig. 5) following the profile approach (black, Table 3) and compartment approach (blue), using the local upper (z_c), active (z_a) and lower (z_*) shoreface limits as closure depth (Table 2). Shoreline change is measured landward from the edge of the beach fluctuation zone (dashed red) and thus R represents predicted future foredune crest positions



shoreline change for open-coast NSW beaches with an aim to identify the full potential range of exposure to coastal erosion at present and in the future. They developed a preliminary compartment classification based on navigation bathymetry to guide modelling. In the absence of detailed shoreface seabed mapping, they assumed that the active zone extended between regional-scale values of z_b and z_* and was uniformly sand, and that projected sea level rise would generate sediment accommodation across the active zone in all settings. Our investigation of shoreface geomorphology and morphodynamics in the Illawarra South compartment, however, shows that shoreline change in response to sea level rise may be strongly influenced by shoreface variability at the sub-compartment scale. In the Perkins-Windang tertiary compartment, our findings suggest that the future sediment budget may be influenced by a restricted Bruun effect (response limited to the upper shoreface and the Perkins sub-compartment active zone only) and potential

ongoing sand supplies from a lower shoreface-inner shelf sand body (Perkins sub-compartment) and ebb-delta sediment lobe (Windang sub-compartment). Simply applying the profile approach to shoreline change prediction using high-resolution seabed mapping is thus inadequate and potentially misleading. Instead, high-resolution mapping should be applied within compartment-based modelling frameworks to improve future shoreline change forecasts.

Conclusions

High-resolution mapping and sampling of the Illawarra South compartment shoreface-inner shelf has revealed seabed geomorphology and sediment distributions that are more complex than previously known, providing new insights on local-scale variability within the context of regional-scale and depth-based shelf

sedimentation models for our region. Detailed seabed mapping in shallow coastal waters enables more accurate definition of sediment connectivity and dynamics using a compartment framework and is a critical step towards developing quantitative sediment budgets that can underpin locally meaningful predictions of future shoreline change under projected climate change scenarios. This is particularly true for embayed and accommodation-dominated coastal settings with limited sediment supply. High-resolution seabed mapping and characterisation reduces unnecessary epistemic uncertainty in shoreline change predictions emerging from common assumptions about shoreface morphology and morphodynamics in the absence of readily attainable data. By advancing the knowledge base through fundamental data collection and analysis, we can increase confidence in shoreline change forecasts, improving evidence-based decision-making in coastal risk management and planning.

The morphodynamic state of the shoreface and the timescale-dependent extent of morphodynamic response (the active zone) may be critical determinants of shoreline response to sea level rise. By comparing detailed seabed mapping data with shoreface equilibrium geometry and critical limiting depths predicted using wave-driven sediment transport theory and local wave climate data, shoreface morphodynamics can be assessed at a local scale. This enables evaluation of both underlying and potential sediment exchanges between the shoreface and beach (and resulting shoreline change), which may arise from ongoing shoreface response to the inherited depositional conditions and relative sea level change. Our analysis revealed some notable correlation between predicted and observed shoreface geometry, and between predicted shoreface limiting depths and depositional evidence (sediment distributions), which affords some confidence in the predictive methods. While we provide a simple example of the potential improvements to shoreline change prediction that high-resolution seabed mapping and compartment parameterisation enables, fully quantitative compartment sediment budgets based on detailed seabed (and sub-surface) mapping and sediment transport modelling remain the ultimate goal to advance shoreline change prediction in our setting.

Acknowledgements The authors thank Fugro Australia Pty. Ltd. for the lidar data acquisition and processing, and Jeff Miller, Master of *RV Bombora*. The two anonymous reviewers provided thoughtful and constructive feedback that greatly improved this manuscript.

Funding Information Seabed mapping was funded through the New South Wales Government Coastal Reforms funding package and Climate Change Fund. Laboratory sediment analyses were funded through a SMAH Research Partnership Grant between the Office of Environment and Heritage (now Department of Planning, Industry and Environment) and the University of Wollongong: Sediment dynamics and stability of the Illawarra coast (2017).

Open Access This article is licensed under a Creative Commons Attribution 4.0 International License, which permits use, sharing, adaptation, distribution and reproduction in any medium or format, as long as you give appropriate credit to the original author(s) and the

source, provide a link to the Creative Commons licence, and indicate if changes were made. The images or other third party material in this article are included in the article's Creative Commons licence, unless indicated otherwise in a credit line to the material. If material is not included in the article's Creative Commons licence and your intended use is not permitted by statutory regulation or exceeds the permitted use, you will need to obtain permission directly from the copyright holder. To view a copy of this licence, visit <http://creativecommons.org/licenses/by/4.0/>.

References

- Aagaard, T., and M.G. Hughes. 2017. Equilibrium shoreface profiles: A sediment transport approach. *Marine Geology* 390: 321–330. <https://doi.org/10.1016/j.margeo.2016.12.013>.
- Bagnold, R.A. 1963. Mechanics of marine sedimentation. In *Physics of sediment transport by wind and water*, ed. M.N. Hill, 188–230. New York: John Wiley.
- Barbier, E.B., S.D. Hacker, C. Kennedy, E.W. Kock, A.C. Stier, and B.R. Sillman. 2011. The value of estuarine and coastal ecosystem services. *Ecological Monographs* 81 (2): 169–193. <https://doi.org/10.1890/10-1510.1>.
- Blott, S.J., and K. Pye. 2001. GRADISTAT: A grain size distribution and statistics package for the analysis of unconsolidated sediments. *Earth Surface Process and Landforms* 26 (11): 1237–1248.
- Bowen, A.J. 1980. Simple models of nearshore sedimentation, beach profiles and longshore bars. In *The Coastline of Canada, Littoral Processes and Shore Morphology*, ed. S.B. McCann. Geological Survey of Canada. <https://doi.org/10.4095/102213>.
- Boyd, R., K. Ruming, and J.J. Roberts. 2004. Geomorphology and surficial sediments of the southeast Australian continental margin. *Australian Journal of Earth Sciences* 51 (5): 743–764. <https://doi.org/10.1111/j.1400-0952.2004.01086.x>.
- Brenner, O.T., L.J. Moore, and A.B. Murray. 2015. The complex influences of back-barrier deposition, substrate slope and underlying stratigraphy in barrier island response to sea-level rise: Insights from the Virginia Barrier Islands, Mid-Atlantic Bight, U.S.A. *Geomorphology* 246: 334–350. <https://doi.org/10.1016/j.geomorph.2015.06.014>.
- Brenner, O.T., E.E. Lentz, C.J. Hapke, R.E. Henderson, K.E. Wilson, and T.R. Nelson. 2018. Characterizing storm response and recovery using the beach change envelope: Fire Island, New York. *Geomorphology* 300:189–202. <https://doi.org/10.1016/j.geomorph.2017.08.004>.
- Bruun, P. 1962. Sea level rise as a cause of shore erosion. *Journal of Waterways and Harbors Division, ASCE* 88: 117–130.
- Bruun, P. 1983. Review of conditions for uses of the Bruun Rule of erosion. *Coastal Engineering* 7 (1): 77–89. [https://doi.org/10.1016/0378-3839\(83\)90028-5](https://doi.org/10.1016/0378-3839(83)90028-5).
- Bruun, P. 1988. The Bruun Rule of erosion by sea-level rise - a discussion on large-scale two- and three-dimensional usages. *Journal of Coastal Research* 4: 627–648.
- Cardno. (2010). Wollongong City Council Coastal Zone Study. Report prepared for Wollongong City Council. 83pp.
- Carvalho, R., M. Kinsela, D. Hanslow, S. Hamylton, M. Linklater, T. Ingleton, B. Morris, K. Allen, and C. Woodroffe. 2017. Identifying sediment compartment dynamics on the Illawarra coast. In *Proceedings of the 26th NSW Coastal Conference*, Port Stephens.
- Castelle, B., V. Marieu, S. Bujan, K.D. Splinter, A. Robinet, N. Sénéchal, and S. Ferreira. 2015. Impact of the winter 2013–2014 series of severe Western Europe storms on a double-barred sandy coast: Beach and dune erosion and megacusp embayments. *Geomorphology* 238: 135–148. <https://doi.org/10.1016/j.geomorph.2015.03.006>.

- Cechet, R., M. Hazelwood, D. Skene, C. Griffin, M. Dunford, L. Power, S. Canterford, K. Nadimpalli, P. Taylor, M. Woolf, and H. Anderson. 2012. Impacts of climate change on human settlements and other nationally significant infrastructure in the coastal zone. Record 2012/65. Geoscience Australia: Canberra, 46p. <https://pid.geoscience.gov.au/dataset/ga/74658>.
- Chapman, D.M., M. Geary, P.S. Roy, and B.G. Thom. 1982. *Coastal evolution and coastal erosion in New South Wales*. Coastal Council of New South Wales: Sydney.
- Clarke, D.J., and I.G. Eliot. 1988. Low-frequency changes of sediment volume on the beachface at Warilla Beach, New South Wales, 1975–1985. *Marine Geology* 79 (3–4): 189–211. [https://doi.org/10.1016/0025-3227\(88\)90039-4](https://doi.org/10.1016/0025-3227(88)90039-4).
- Cooper, J.A.G., and O.H. Pilkey. 2004. Sea-level rise and shoreline retreat: Time to abandon the Bruun Rule. *Global and Planetary Change* 43 (3–4): 157–171. <https://doi.org/10.1016/j.gloplacha.2004.07.001>.
- Cooper, N.J., and N.I. Pontee. 2006. Appraisal and evolution of the littoral “sediment cell” concept in applied coastal management: Experiences from England and Wales. *Ocean & Coastal Management* 49 (7–8): 498–510. <https://doi.org/10.1016/j.ocecoaman.2006.04.003>.
- Cooper, J.A.G., A.N. Green, and C. Loureiro. 2018. Geological constraints on mesoscale coastal barrier behaviour. *Global and Planetary Change* 168: 15–34. <https://doi.org/10.1016/j.gloplacha.2018.06.006>.
- Cooper, J.A.G., G. Masselink, G. Coco, A.D. Short, B. Castelle, K. Rogers, E. Anthony, A.N. Green, J.T. Kelley, O.H. Pilkey, and D.W.T. Jackson. 2020. Sandy beaches can survive sea-level rise. *EarthArXiv* March 18. <https://doi.org/10.31223/osf.io/4md6e>.
- Cowell, P.J., and M.A. Kinsela. 2018. Shoreface controls on barrier evolution and shoreline change. In *Barrier dynamics and response to changing climate*, ed. L.J. Moore and A.B. Murray, 243–275. Springer International. <https://doi.org/10.1007/978-3-319-68086-6>.
- Cowell, P.J., and B.G. Thom. 1994. Morphodynamics of coastal evolution. In *Coastal evolution: Late Quaternary shoreline morphodynamics*, ed. R.W.G. Carter and C.D. Woodroffe, 33–86. Cambridge: Cambridge University Press.
- Cowell, P.J., P.S. Roy, and R.A. Jones. 1995. Simulation of large-scale coastal change using a morphological behavior model. *Marine Geology* 126 (1–4): 45–61. [https://doi.org/10.1016/0025-3227\(95\)00065-7](https://doi.org/10.1016/0025-3227(95)00065-7).
- Cowell, P.J., D.J. Hanslow, and J.F. Meleo. 1999. The shoreface. In *Handbook of beach and shoreface morphodynamics*, ed. A.D. Short. New York: John Wiley.
- Cowell, P.J., M.J.F. Stive, A.W. Niedoroda, H.J. de Vriend, D.J.P. Swift, G.M. Kaminsky, and M. Capobianco. 2003a. The coastal-tract (part 1): A conceptual approach to aggregated modeling of low-order coastal change. *Journal of Coastal Research* 19: 812–827.
- Cowell, P.J., M.J.F. Stive, A.W. Niedoroda, D.J.P. Swift, H.J. de Vriend, M.C. Buijsman, R.J. Nicholls, et al. 2003b. The coastal-tract (part 2): Applications of aggregated modeling of lower-order coastal change. *Journal of Coastal Research* 19: 828–848.
- Cowell, P.J., B.G. Thom, R.A. Jones, C.H. Everts, and D. Simanovic. 2006. Management of uncertainty in predicting climate-change impacts on beaches. *Journal of Coastal Research* 22: 232–245. <https://doi.org/10.2112/05A-0018.1>.
- Curry, J.R. 1964. Transgressions and regressions. In *Papers in marine geology*, ed. R.L. Miller, 175–203. New York: Macmillan.
- Daley, M.J.A. and P.J. Cowell. 2013. Long-term shoreface response to disequilibrium-stress: A conundrum for climate change. In *Proceedings of the 22nd NSW Coastal Conference*, Port Macquarie.
- Dean, R.G. 1991. Equilibrium beach profiles - characteristics and applications. *Journal of Coastal Research* 7: 53–84.
- Doyle, T.B., A.D. Short, and C.D. Woodroffe. 2019a. Fore-dune evolution in eastern Australia: A management case study on Warilla Beach. In *Coastal Sediments 2019: Proceedings of the 9th International Conference*, 2309–2324. Tampa: World Scientific. <https://doi.org/10.1142/11391>.
- Doyle, T.B., A.D. Short, P. Ruggiero, and C.D. Woodroffe. 2019b. Interdecadal fore-dune changes along the Southeast Australian Coastline: 1942–2014. *Journal of Marine Science and Engineering* 7 (6): 177. <https://doi.org/10.3390/jmse7060177>.
- Ferland, M.A., 1990. Shelf sand bodies in Southeastern Australia. Sydney: The University of Sydney, unpublished PhD thesis.
- Field, M.E., and P.S. Roy. 1984. Offshore transport and sand-body formation - evidence from a steep, high-energy shoreface, southeastern Australia. *Journal of Sedimentary Petrology* 54: 1292–1302.
- Finkl, C.W., L. Benedet, and J.L. Andrews. 2005. Interpretation of seabed geomorphology based on spatial analysis of high-density airborne laser bathymetry. *Journal of Coastal Research* 21: 501–514. <https://doi.org/10.2112/05-756A.1>.
- FitzGerald, D.M., M.S. Fenster, B.A. Argow, and I.V. Buynevich. 2008. Coastal impacts due to sea-level rise. In *Annual review of earth and planetary sciences*, 36:601–647. Palo Alto: Annual Reviews. <https://doi.org/10.1146/annurev.earth.35.031306.140139>.
- Folk, R.L., and W.C. Ward. 1957. Brazos River bar: A study in the significance of grain size parameters. *Journal of Sedimentary Research* 27 (1): 3–26.
- French, J., H. Burningham, G. Thornhill, R. Whitehouse, and R.J. Nicholls. 2016. Conceptualising and mapping coupled estuary, coast and inner shelf sediment systems. *Geomorphology* 256: 17–35. <https://doi.org/10.1016/j.geomorph.2015.10.006>.
- FrontierSI. 2019. QA4LIDAR: Quick and Accurate Quality Assurance of Airborne LiDAR. <https://qa4lab.com/qa4lidar/>
- Fruergaard, M., P.N. Johannessen, L.H. Nielsen, L. Nielsen, I. Møller, T.J. Andersen, S. Piasecki, and M. Pejrup. 2018. Sedimentary architecture and depositional controls of a Holocene wave-dominated barrier-island system. *Sedimentology* 65 (4): 1170–1212. <https://doi.org/10.1111/sed.12418>.
- Goodwin, I.D., R. Freeman, and K. Blackmore. 2013. An insight into headland sand bypassing and wave climate variability from shoreface bathymetric change at Byron Bay, New South Wales, Australia. *Marine Geology* 341: 29–45. <https://doi.org/10.1016/j.margeo.2013.05.005>.
- Hallermeier, R.J. 1981. A profile zonation for seasonal sand beaches from wave climate. *Coastal Engineering* 4: 253–277. [https://doi.org/10.1016/0378-3839\(80\)90022-8](https://doi.org/10.1016/0378-3839(80)90022-8).
- Hanslow, D.J. 2007. Beach erosion trend measurement: A comparison of trend indicators. *Journal of Coastal Research* SI50: 588–593.
- Hanslow, D.J., J. Dela-Cruz, B.D. Morris, M.A. Kinsela, E. Foulsham, M. Linklater, and T.R. Pritchard. 2016. Regional scale coastal mapping to underpin strategic land use planning in south east Australia. *Journal of Coastal Research* SI75: 987–991. <https://doi.org/10.2112/SI75-198.1>.
- Hanslow, D.J., B.D. Morris, E. Foulsham, and M.A. Kinsela. 2018. A regional scale approach to assessing current and potential future exposure to tidal inundation in different types of estuaries. *Scientific Reports* 8 (1): 7065. <https://doi.org/10.1038/s41598-018-25410-y>.
- Harley, M.D., I.L. Turner, M.A. Kinsela, J.H. Middleton, P.J. Mumford, K.D. Splinter, M.S. Phillips, J.A. Simmons, D.J. Hanslow, and A.D. Short. 2017. Extreme coastal erosion enhanced by anomalous extratropical storm wave direction. *Scientific Reports* 7 (1): 6033. <https://doi.org/10.1038/s41598-017-05792-1>.
- Harrison, A.J., B.M. Miller, J.T. Carley, I.L. Turner, R. Clout, and B. Coates. 2017. NSW Beach photogrammetry: A new, online database and toolbox. In *Proceedings of the Australasian Coasts & Ports Conference 2017*, Cairns.
- Hart, R.M., H.E. Power, and D.J. Hanslow (2017). Tidal dynamics and oscillations within coastal lakes. In *Proceedings of the Australasian Coasts & Ports Conference 2017*, Cairns.

- Inman, D.L., M.H.S. Elwany, and S.A. Jenkins. 1993. Shorerise and berm profiles on ocean beaches. *Journal of Geophysical Research-Oceans* 98 (C10): 18181–18199. <https://doi.org/10.1029/93JC00996>.
- Kennedy, D.M., D. Ierodiaconou, and A. Schimel. 2014. Granitic coastal geomorphology: Applying integrated terrestrial and bathymetric LiDAR with multibeam sonar to examine coastal landscape evolution. *Earth Surface Processes and Landforms* 39: 1663–1674. <https://doi.org/10.1002/esp.3615>.
- Kinsela, M.A., and D.J. Hanslow. 2013. Coastal erosion risk assessment in New South Wales: Limitations and future directions. In *Proceedings of the 22nd NSW Coastal Conference*, Port Macquarie.
- Kinsela, M.A., M.J.A. Daley, and P.J. Cowell. 2016. Origins of Holocene coastal strandplains in Southeast Australia: Shoreface sand supply driven by disequilibrium morphology. *Marine Geology* 374: 14–30. <https://doi.org/10.1016/j.margeo.2016.01.010>.
- Kinsela, M.A., B.D. Morris, M. Linklater, and D.J. Hanslow. 2017. Second-pass assessment of potential exposure to shoreline change in New South Wales, Australia, using a sediment compartments framework. *Journal of Marine Science and Engineering* 5 (4): 61. <https://doi.org/10.3390/jmse5040061>.
- Komar, P.D. 1996. The budget of littoral sediments: Concepts and applications. *Shore & Beach* 64: 18–26.
- Lazarus, E.D., M.A. Ellis, A.B. Murray, and D.M. Hall. 2016. An evolving research agenda for human-coastal systems. *Geomorphology* 256: 81–90. <https://doi.org/10.1016/j.geomorph.2015.07.043>.
- Le Cozannet, G., J.-C. Manceau, and J. Rohmer. 2017. Bounding probabilistic sea-level projections within the framework of the possibility theory. *Environmental Research Letters* 12 (1): 014012. <https://doi.org/10.1088/1748-9326/aa5528>.
- Linklater, M., T.C. Ingleton, M.A. Kinsela, B.D. Morris, K.M. Allen, M.D. Sutherland, and D.J. Hanslow. 2019. Techniques for classifying seabed morphology and composition on a subtropical-temperate continental shelf. *Geosciences* 9 (3): 141. <https://doi.org/10.3390/geosciences9030141>.
- Lorenzo-Trueba, J., and A.D. Ashton. 2014. Rollover, drowning, and discontinuous retreat: Distinct modes of barrier response to sea-level rise arising from a simple morphodynamic model. *Journal of Geophysical Research: Earth Surface* 119 (4): 779–801. <https://doi.org/10.1002/2013JF002941>.
- Miselis, J.L., and J.E. McNinch. 2006. Calculating shoreline erosion potential using nearshore stratigraphy and sediment volume: Outer Banks, North Carolina. *Journal of Geophysical Research: Earth Surface* 111: F02019. <https://doi.org/10.1029/2005JF000389>.
- Nicholls, R.J., and A. Cazenave. 2010. Sea-level rise and its impact on coastal zones. *Science* 328 (5985): 1517–1520. <https://doi.org/10.1126/science.1185782>.
- Nicholls, R.J., W.A. Birkemeier, and G.H. Lee. 1998. Evaluation of depth of closure using data from Duck, NC, USA. *Marine Geology* 148 (3–4): 179–201. [https://doi.org/10.1016/S0025-3227\(98\)00011-5](https://doi.org/10.1016/S0025-3227(98)00011-5).
- Niederoda, A.W., D.J.P. Swift, T.S. Hopkins, and C.M. Ma. 1984. Shoreface morphodynamics on wave-dominated coasts. *Marine Geology* 60 (1–4): 331–354. [https://doi.org/10.1016/0025-3227\(84\)90156-7](https://doi.org/10.1016/0025-3227(84)90156-7).
- Oppenheimer, M., B.C. Glavovic, J. Hinkel, R. van de Wal, A.K. Magnan, A. Abd-Elgawad, R. Cai, M. Cifuentes-Jara, R.M. DeConto, T. Ghosh, J. Hay, F. Isla, B. Marzeion, B. Meyssignac, and Z. Sebesvari. 2019. Sea level rise and implications for low-lying islands, coasts and communities. In *IPCC special report on the ocean and cryosphere in a changing climate* ed. H.-O. Pörtner, D.C. Roberts, V. Masson-Delmotte, P. Zhai, M. Tignor, E. Poloczanska, K. Mintenbeck, A. Alegría, M. Nicolai, A. Okem, J. Petzold, B. Rama, N.M. Weyer.
- Ortiz, A.C., and A.D. Ashton. 2016. Exploring shoreface dynamics and a mechanistic explanation for a morphodynamic depth of closure. *Journal of Geophysical Research: Earth Surface* 121 (2): 442–464. <https://doi.org/10.1002/2015JF003699>.
- Patterson, D.C., and P. Nielsen. 2016. Depth, bed slope and wave climate dependence of long term average sand transport across the lower shoreface. *Coastal Engineering* 117: 113–125. <https://doi.org/10.1016/j.coastaleng.2016.07.007>.
- Pilkey, O.H., R.S. Young, S.R. Riggs, A.W.S. Smith, H.Y. Wu, and W.D. Pilkey. 1993. The concept of shoreface profile of equilibrium - a critical review. *Journal of Coastal Research* 9: 255–278.
- Rosati, J.D. 2005. Concepts in sediment budgets. *Journal of Coastal Research* 21: 307–322. <https://doi.org/10.2112/02-475A.1>.
- Roy, P.S. 2006. *Inner continental shelf sand deposits: SE Australia*. Sydney: University of Sydney Institute of Marine Science and School of Geoscience.
- Roy, P.S., and A.W. Stephens. 1980. Geological controls on process-response, SE Australia. In *Coastal Engineering 1980: Proceedings of the 17th International Conference on Coastal Engineering*, 913–933. <https://doi.org/10.1061/9780872622647.057>.
- Roy, P.S., and B.G. Thom. 1981. Late Quaternary marine deposition in New South Wales and southern Queensland - an evolutionary model. *Journal of the Geological Society of Australia* 28 (3–4): 471–489.
- Roy, P.S., P.J. Cowell, M.A. Ferland, and B.G. Thom. 1994. Wave dominated coasts. In *Coastal evolution: Late Quaternary shoreline morphodynamics*, ed. R.W.G. Carter and C.D. Woodroffe, 121–186. Cambridge: Cambridge University Press.
- Schwab, W.C., W.E. Baldwin, C.J. Hapke, E.E. Lentz, P.T. Gayes, J.F. Denny, J.H. List, and J.C. Warner. 2013. Geologic evidence for onshore sediment transport from the inner continental shelf: Fire Island, New York. *Journal of Coastal Research* 288: 526–544. <https://doi.org/10.2112/JCOASTRES-D-12-00160.1>.
- Scott, T., G. Masselink, T. O'Hare, A. Saulter, T. Poate, P. Russell, M. Davidson, and D. Conley. 2016. The extreme 2013/2014 winter storms: Beach recovery along the southwest coast of England. *Marine Geology* 382: 224–241. <https://doi.org/10.1016/j.margeo.2016.10.011>.
- Short, A.D. 2007. *Beaches of the New South Wales coast*. 2nd ed. Sydney: Sydney University Press.
- Short, A.D. 2020. *Australian coastal systems: beaches, barriers and sediment compartments*, Coastal Research Library 32. Switzerland: Springer. <https://doi.org/10.1007/978-3-030-14294-0>.
- Simeone, S., E. Molinaroli, A. Conforti, and G. De Falco. 2018. Impact of ocean acidification on the carbonate sediment budget of a temperate mixed beach. *Climatic Change* 150 (3–4): 227–242. <https://doi.org/10.1007/s10584-018-2282-3>.
- SMEC. 2010. Shellharbour coastal hazard analysis. Report prepared for Shellharbour City Council. 55pp.
- Stive, M.J.F. 2004. How important is global warming for coastal erosion? An editorial comment. *Climatic Change* 64 (1/2): 27–39. <https://doi.org/10.1023/B:CLIM.0000024785.91858.1d>.
- Stive, M.J.F., and H.J. de Vriend. 1995. Modeling shoreface profile evolution. *Marine Geology* 126 (1–4): 235–248. [https://doi.org/10.1016/0025-3227\(95\)00080-1](https://doi.org/10.1016/0025-3227(95)00080-1).
- Sweet, W.V., R.E. Kopp, C.P. Weaver, J. Obeysekera, R.M. Horton, E.R. Thieler, and C. Zervas. 2017. *Global and regional sea level rise scenarios for the United States*. National Oceanic and Atmospheric Administration (NOAA): Silver Spring.
- Swift, D.J.P., S. Phillips, and J.A. Thorne. 1991. Sedimentation on continental margins IV: Lithofacies and depositional systems. In *Shelf sand and sandstone bodies - geometry, facies and sequence stratigraphy*, ed. D.J.P. Swift, G.F. Oertel, R.W. Tillman, and J.A. Thorne, 89–152. Oxford: Blackwell Scientific Publications.
- Taylor, D., S. Garber, J. Burston, E. Couriel, B. Modra, and M. Kinsela. 2015. Verification of a coastal wave transfer function for the New South Wales coastline. In *Proceedings of the Australian Coasts and Ports Conference 2015*, Auckland.

- Thieler, E.R., A.L. Brill, W.J. Cleary, C.H. Hobbs, and R.A. Gammisch. 1995. Geology of the Wrightsville Beach, North-Carolina shoreface - implications for the concept of shoreface profile of equilibrium. *Marine Geology* 126 (1-4): 271–287. [https://doi.org/10.1016/0025-3227\(95\)00082-A](https://doi.org/10.1016/0025-3227(95)00082-A).
- Thieler, E.R., O.H. Pilkey, R.S. Young, D.M. Bush, and F. Chai. 2000. The use of mathematical models to predict beach behavior for US coastal engineering: A critical review. *Journal of Coastal Research* 16: 48–70.
- Thieler, E.R., O.H. Pilkey, W.J. Cleary, and W.C. Schwab. 2001. Modern sedimentation on the shoreface and inner continental shelf at Wrightsville Beach, North Carolina, U.S.A. *Journal of Sedimentary Research* 71 (6): 958–970. <https://doi.org/10.1306/032101710958>.
- Thom, B.G., J.B. Keene, P.J. Cowell, and M. Daley. 2010. East Australian marine abrasion surface. In *Australian landscapes*, ed. P. Bishop and B. Pillans, vol. 346, 57–69. London: Geological Society. Special Publication. <https://doi.org/10.1144/SP346.5>.
- Thom, B.G., I. Eliot, M. Eliot, N. Harvey, D. Rissik, C. Sharples, A.D. Short, and C.D. Woodroffe. 2018. National sediment compartment framework for Australian coastal management. *Ocean & Coastal Management* 154: 103–120. <https://doi.org/10.1016/j.ocecoaman.2018.01.001>.
- Van Goor, M.A., T.J. Zitman, Z.B. Wang, and M.J.F. Stive. 2003. Impact of sea-level rise on the morphological equilibrium state of tidal inlets. *Marine Geology* 202 (3-4): 211–227. [https://doi.org/10.1016/S0025-3227\(03\)00262-7](https://doi.org/10.1016/S0025-3227(03)00262-7).
- Van Maanen, B., G. Coco, K.R. Bryan, and C.T. Friedrichs. 2013. Modeling the morphodynamic response of tidal embayments to sea-level rise. *Ocean Dynamics* 63 (11-12): 1249–1262. <https://doi.org/10.1007/s10236-013-0649-6>.
- Wainwright, D.J., R. Ranasinghe, D.P. Callaghan, C.D. Woodroffe, P.J. Cowell, and K. Rogers. 2014. An argument for probabilistic coastal hazard assessment: Retrospective examination of practice in New South Wales, Australia. *Ocean and Coastal Management* 95: 147–155. <https://doi.org/10.1016/j.ocecoaman.2014.04.009>.
- Walters, D., L.J. Moore, O. Duran Vinent, S. Fagherazzi, and G. Mariotti. 2014. Interactions between barrier islands and backbarrier marshes affect island system response to sea level rise: Insights from a coupled model. *Journal of Geophysical Research: Earth Surface* 119: 2013–2031. <https://doi.org/10.1002/2014JF003091>.
- Wiecek, D., C. Regena, R. Laine, and R.J. Williams. 2016. Quantifying change and impacts to Lake Illawarra from a permanent opening. In *Proceedings of the 25th NSW Coastal Conference*, Coffs Harbour.
- Wolinsky, M.A., and A.B. Murray. 2009. A unifying framework for shoreline migration: 2. Application to wave-dominated coasts. *Journal of Geophysical Research: Earth Surface* 114: F01009. <https://doi.org/10.1029/2007JF000856>.
- Wright, L.D. 1995. *Morphodynamics of inner continental shelves*. Boca Raton: CRC.
- Young, S., E. Couriel, I. Jayawardene, B. McPherson, and B. Dooley. 2014. Case study: Assessment of the entrance stability of the Lake Illawarra estuary. *Australian Journal of Civil Engineering* 12: 41–52.
- Zhang, K., B.C. Douglas, and S.P. Leatherman. 2004. Global warming and coastal erosion. *Climatic Change* 64 (1/2): 41–58. <https://doi.org/10.1023/B:CLIM.0000024690.32682.48>.